NASA/TM—2001-210578

Deformation and Life Analysis of Composite Flywheel Disk and Multi-Disk Systems

S.M. Arnold
Glenn Research Center, Cleveland, Ohio

A.F. Saleeb and N.R. Al-Zoubi
University of Akron, Akron, Ohio

January 2001

Since its founding, NASA has been dedicated to the advancement of aeronautics and space science. The NASA Scientific and Technical Information (STI) Program Office plays a key part in helping NASA maintain this important role.

The NASA STI Program Office is operated by Langley Research Center, the Lead Center for NASA's scientific and technical information. The NASA STI Program Office provides access to the NASA STI Database, the largest collection of aeronautical and space science STI in the world. The Program Office is also NASA's institutional mechanism for disseminating the results of its research and development activities. These results are published by NASA in the NASA STI Report Series, which includes the following report types:

- TECHNICAL PUBLICATION. Reports of completed research or a major significant phase of research that present the results of NASA programs and include extensive data or theoretical analysis. Includes compilations of significant scientific and technical data and information deemed to be of continuing reference value. NASA's counterpart of peer-reviewed formal professional papers but has less stringent limitations on manuscript length and extent of graphic presentations.

- TECHNICAL MEMORANDUM. Scientific and technical findings that are preliminary or of specialized interest, e.g., quick release reports, working papers, and bibliographies that contain minimal annotation. Does not contain extensive analysis.

- CONTRACTOR REPORT. Scientific and technical findings by NASA-sponsored contractors and grantees.

- CONFERENCE PUBLICATION. Collected papers from scientific and technical conferences, symposia, seminars, or other meetings sponsored or cosponsored by NASA.

- SPECIAL PUBLICATION. Scientific, technical, or historical information from NASA programs, projects, and missions, often concerned with subjects having substantial public interest.

- TECHNICAL TRANSLATION. English-language translations of foreign scientific and technical material pertinent to NASA's mission.

Specialized services that complement the STI Program Office's diverse offerings include creating custom thesauri, building customized data bases, organizing and publishing research results . . . even providing videos.

For more information about the NASA STI Program Office, see the following:

- Access the NASA STI Program Home Page at *http://www.sti.nasa.gov*

- E-mail your question via the Internet to help@sti.nasa.gov

- Fax your question to the NASA Access Help Desk at 301–621–0134

- Telephone the NASA Access Help Desk at 301–621–0390

- Write to:
  NASA Access Help Desk
  NASA Center for AeroSpace Information
  7121 Standard Drive
  Hanover, MD 21076

Deformation and Life Analysis of Composite Flywheel Disk and Multi-Disk Systems

S.M. Arnold
Glenn Research Center, Cleveland, Ohio

A.F. Saleeb and N.R. Al-Zoubi
University of Akron, Akron, Ohio

Acknowledgments

The authors would like to thank Jeff Trudell for his assistance in supplying the FEA validation results and for his many helpful suggestions during the review of this manuscript.

DEFORMATION AND LIFE ANALYSIS OF COMPOSITE FLYWHEEL DISK AND MULTI-DISK SYSTEMS

S. M. Arnold
National Aeronautics and Space Administration
Glenn Research Center
Cleveland, Ohio 44135

A. F. Saleeb and N. R. Al-Zoubi
University of Akron
Akron, Ohio 44325

SUMMARY

In this study an attempt is made to put into perspective the problem of a rotating disk, be it a single disk or a number of concentric disks forming a unit. An analytical model capable of performing an elastic stress analysis for single/multiple, annular/solid, anisotropic/isotropic disk systems, subjected to both pressure surface tractions, body forces (in the form of temperature-changes and rotation fields) and interfacial misfits is derived and discussed. Results of an extensive parametric study are presented to clearly define the key design variables and their associated influence. In general the important parameters were identified as misfit, mean radius, thickness, material property and/or load gradation, and speed; all of which must be simultaneously optimized to achieve the "best" and most reliable design. Also, the important issue of defining proper performance/merit indices (based on the specific stored energy), in the presence of multiaxiality and material anisotropy is addressed. These merit indices are then utilized to discuss the difference between flywheels made from PMC and TMC materials with either an annular or solid geometry.

Finally two major aspects of failure analysis, that is the static and cyclic limit (burst) speeds are addressed. In the case of static limit loads, upper, lower, and out-of-plane bounds for disks with constant thickness are presented for both the case of internal pressure loading (as one would see in a hydroburst test) and pure rotation (as in the case of a free spinning disk). The results (interaction diagrams) are displayed graphically in designer friendly format. For the case of fatigue, a representative fatigue/life master curve is illustrated in which the normalized limit speed versus number of applied cycles is given for a cladded TMC disk application.

SYMBOLS

Material Parameters

E_L	longitudinal Young's modulus
E_T	transverse Young's modulus
K	transverse yield stress under shear loading
α_L	longitudinal thermal expansion
α_T	transverse thermal expansion
β	ratio of anisotropy, i.e., $\left(\dfrac{E_T}{E_L}\right)$
ν_L	longitudinal Poisson's ratio, i.e., $(\varepsilon_r/\varepsilon_\theta$, load is in θ direction)
ξ	ratio of longitudinal to transverse ultimate stresses, i.e., $\left(\dfrac{\sigma_{u_L}}{\sigma_{u_T}}\right)$
ρ	material density
$\sigma_{u_L}, \sigma_{u_T}$	ultimate tensile strength (UTS) in the longitudinal and transverse directions respectively.
σ_L^Y	longitudinal yield stress

Stresses and Strains

D_{ij}	second order direction tensor
d_i	unit vector denoting local fiber direction
$F(\ )$	limit function (static fracture, endurance limit and normalization surfaces)
S_{ij}	deviatoric stress tensor
σ_{ij}	Cauchy stress tensor
σ_r, ε_r	radial stress and strain components respectively
$\sigma_\theta, \varepsilon_\theta$	tangential stress and strain components respectively

Subscripts and Superscripts

$(\ )_L, (\ )_T$	longitudinal and transverse properties (static fracture, endurance limit and normalization surfaces) respectively
$(\bullet)$	denotes differential with respect to time

Geometry

a	inner radius
b	outer radius
h	height
R_m	mean radius
R_i	radial location of the ith interface
r	radius
u	radial deflection
δ	misfit between concentric disks
λ	width of a given disk

Forces

P_{in}	internal applied pressure
P_{out}	external applied pressure
$\hat{P}$	Generalized Pressure Loading: (a) When internal pressure loading applied; equal to internal pressure P_{in} (b) When rotational loading is applied; equal to the equivalent centripetal pressure load, i.e., $\hat{P} = \rho\omega^2 (b^2 - a^2)/2$
T_a	temperature at the inner diameter, r = a
T_b	temperature at the outer diameter, r = b
ΔT	radial temperature distribution
ω	speed of rotation

1.0 INTRODUCTION

1.1 General

Over the years, there has been an increasing demand for effective energy storing systems (ref. 1). To meet such needs, many alternative systems have been proposed, as listed in table I, with composite flywheel energy storage systems rising to the top of the list of candidates, because of there high power and energy densities with no fall-off

in capacity under repeated charge-discharge cycles. In recent years, a host (e.g., refs. 1 to 3) of different flywheel system designs (composed of various fiber-reinforced material systems, i.e., metallic composites, polymeric composites, etc.) have been identified with the goal of improving the performance of these systems. These flywheel systems can be categorized into principally three design topologies: (1) preloaded, (2) growth matching, and (3) mass loaded, with each approach having its own set of advantages and disadvantages.

Energy storage in all these flywheel designs is basically sustained by a spinning mass, called a rotor. This important "rotor" component has therefore been the subject of research investigations over many years, generating extensive literature on its many analysis and design related aspects. At different stages of developments, a number of comprehensive state-of-art reviews (refs. 1 and 2) have been completed. For instance, representatives of these in the area of material-system selections for flywheel devices are given in Genta (ref. 1) and DeTeresa (ref. 4) whereas optimization for integrated system design are given by Bitterly (ref. 3).

In the following section, a brief summary is given for the state-of-art that is presently available on the analysis-related aspects of the rotor-type components (also disks, multiple-disks, etc.). However, we emphasize at the outset that the present review is not intended to be exhaustive; rather we are primarily concerned with works and studies on the important factors that should be considered in any valid assessment of the performance (both at working/service and at limiting operational conditions) of flywheel systems. To this end, we will group the pertinent list of references in tables II to IV according to three major considerations; i.e., (1) factors related to additional loading conditions beyond those of rotation (e.g., internal pressure, temperature, and interference fits, etc.), (2) factors related to material behavior (e.g., isotropic versus anisotropic, elastic versus inelastic, etc.) and (3) factors related to geometry (e.g., uniform versus variable thickness, solid versus annular). This background then puts into perspective the subsequent parametric studies and related conclusions in the later part of the paper.

1.2 Background Literature

Starting as early as 1906 the rotating isotropic disk has been studied by Grubler (ref. 6) followed by Donatch (ref. 7) in 1912. One of the first "modern" dissertations in analyzing the flywheel rotor was the seminal work done by Stodola (ref. 8), whose first translation to English was made in 1917. In 1947 Manson (ref. 9) published a finite difference method to calculate elliptic stresses in gas-turbine disks that could account for the point-to-point variations of disk thickness, temperature, and material properties. Millenson and Manson (ref. 10) extended the method to include plastic flow and creep in 1948. Both methods have been widely used and extended by industry (ref. 11). More recently, Genta (ref. 11) modified Manson's method to include orthotropic materials. The 1960s and 1970s lead to numerous other serious efforts in analyzing the rotor, and introducing different designs for the flywheel, with the onset of composite material development giving added impetus. A detailed review of the rotating disk problem up through the late 1960's is given by Seireg (ref. 12), whereas, Habercom (refs. 13 to 15) provides a collection of abstracts and reference of government-sponsored flywheel related research (late 1960's until the late 1970's). The past 40 years showed a tremendous amount of work done concerning the flywheel, e.g., see Genta's (ref. 11) extensive review, including a historical perspective, on research work conducted up to the early 1980's related specifically to flywheel systems.

For convenience in presentation, we have grouped in tables II and III, respectively, the different representative works with regard to the two major material behavior classifications treated; i.e., elastic-isotropic and elastic anisotropic. These classifications in fact have had a long-standing history in the available literature. The more complex nonlinear counterpart (i.e., plasticity, creep, fracture, etc.) is of more recent origin, and consequently comparatively smaller in size, and primarily focused on isotropic material behavior. A sampling of work on these latter nonlinear areas is given in table IV.

With reference to tables II and III we note that most of the listed investigations have focused on the disk of uniform thickness under rotation. Alternatively, some investigators such as Kaftanoglu (ref. 5), Abir (ref. 41), Huntington (ref. 70), Nimmer (ref. 90), Daniel (ref. 94) and Portnov (ref. 111), considered the effect of misfit in addition to disk rotation as they studied the multirim disk case. Others like Leopold (ref. 18), Potemkina (ref. 31), Prasek (ref. 39), Shanbhag [46], Chakrabarti [61], Gurushankar [66], Dick [74], Baer [82], Misra [100], Ferrero [102] and Portnov (ref. 108), considered the temperature effect as well as the disk rotation case.

Considering the list in table IV, we refer to Shevchenko (ref. 119), Weber (ref. 120), Pisarenko (ref. 121), Reid (ref. 122), Gururaja (ref. 127) and Gueven (ref. 136), for a representative nonlinear elastoplastic analysis of rotating disks, and to Lenard (ref. 147), Gupta (ref. 150), and Mukhopadhyaya (ref. 152), for a number of time-dependent (viscoelastic) solutions.

1.3 Objectives and Outline

In summary, tables II to IV with their broad classification of previous work, convey the complexity of the problem, in that a very large number of conditions and factors must be considered. In particular, each of the listed investigations have necessarily focused on some specified conditions, particular material behavior and related conclusions. An urgent need therefore exists for a compilation, in as concise a form as possible, of the extensive results, major trends observed and the many conclusions reached in these previous studies. To the authors knowledge a study of this type is presently lacking; in which the problem in its "totality" has been considered. As a first step toward this end, an annotative review study is conducted herein, with the major restriction being that of disks with constant thickness. In particular, emphasis is on combined loading (rotation, pressure, misfit, and temperature) and the effect of material anisotropy (with its great impact on stress distributions and any ensuing singularities in stress, strength and failure modes, etc.). To facilitate the presentation of the well-established elastic anisotropic solution procedure (single and multiple disks) specific reference to the numerous previous works cited in tables II and III will not be individually mentioned. However, we emphasis at the outset that all the conclusions made herein are in agreement with these previous works, except of course the notation presently employed. In addition to this review, our second primary objective is to present a number of new analytical and numerical results with regard to limiting conditions of burst (pressure as well as rotation), fatigue, etc. These will then enable us to reach a number of important conclusions in parallel under both service conditions (stress analysis), as well as at the overload conditions for "lifing" studies of the problem.

In an outline form, the remainder of the paper is described as follows. In section II, we give a detailed derivation of the analytical model used in the elastic stress analysis for single/multiple, annular/solid, anisotropic/isotropic disk systems, subjected to both pressure surface tractions, body forces (in the form of temperature-changes and rotation fields) and interfacial misfits. Section III contains the results of extensive parametric studies and important observations obtained therefrom. In Section IV, we address the important issue of defining proper performance/merit indices (based on the specific stored energy), in the presence of anisotropy. Section V deals with two major aspects of failure analysis, i.e., static and cyclic, providing the corresponding limit (burst) load and representative fatigue/life limit speed curve, respectively.

2.0 ELASTIC STRESS ANALYSIS VIA ANALYTICAL MODEL

2.1 Single Disk Solution

2.1.1 Annular Disk.—Here, as classically done the problem of a quasi-static rotating disk subjected to both thermal and mechanical boundary conditions is summarized by stating the governing equations required to define a well-posed boundary value problem. We begin with the equation of equilibrium:

$$\frac{d\sigma_r}{dr} + \frac{\sigma_r - \sigma_\theta}{r} + \rho\omega^2 r = 0 \tag{1}$$

or

$$\sigma_\theta = \frac{d}{dr}(r\sigma_r) + \rho\omega^2 r^2 \tag{2}$$

in which the centrifugal "internal force" $(\rho\omega^2 r)$ is included as a body force term. Next the pertinent compatibility equation,

$$\varepsilon_r = \frac{d}{dr}(r\varepsilon_\theta) \tag{3}$$

is obtained from the well known strain—displacement conditions

$$\varepsilon_r = \frac{du}{dr} \tag{4}$$

and

$$\varepsilon_\theta = \frac{u}{r} \tag{5}$$

so that only the specific constitutive equations to be utilized, need be defined. Given that the problem is an axisymmetric, transversely isotropic disk (with the fiber directed along the circumferential direction of the disk fig. 1), the plane stress constitutive relations are as follows:

$$\varepsilon_r = \frac{\sigma_r}{E_T} - \frac{v_L \sigma_\theta}{E_L} + \alpha_T \Delta T \tag{6}$$

$$\varepsilon_\theta = -\frac{v_L \sigma_r}{E_L} + \frac{\sigma_\theta}{E_L} + \alpha_L \Delta T \tag{7}$$

where ΔT is the assumed linear temperature gradient across the disk and is defined as

$$\Delta T = T_a - T_o + \frac{T_b - T_a}{b - a}(r - a) \tag{8}$$

where a and b define the inner and outer radius of the disk, T_a and T_b are the imposed temperature at the inner and outer radius respectively, and T_o is the reference temperature of the disk.

Substituting the constitutive relations equations (6) and (7) into the compatibility expression, equation (3), and utilizing equilibrium, equation (2); the following governing equation for the radial stress component is obtained:

$$r^2 \frac{d^2\sigma_r}{dr^2} + 3r \frac{d\sigma_r}{dr} + (1 - \frac{1}{\beta})\sigma_r = Q(r) \tag{9}$$

where

$$\beta = \frac{E_T}{E_L} \quad \text{and} \quad Q(r) = \frac{1}{b-a} \begin{bmatrix} rE_L(T_a - T_b)(2\alpha_L - \alpha_T) \\ +a\{E_L(T_b - T_o)(\alpha_L - \alpha_T) + r^2\rho\omega^2(3 + v_L)\} \\ -b\{E_L(T_a - T_o)(\alpha_L - \alpha_T) + r^2\rho\omega^2(3 + v_L)\} \end{bmatrix} \tag{10}$$

Implied in equation (9) is the assumption that the material parameters (i.e., E_L, E_T, v_L, v_T, and G_L, α_L and α_T) are not strongly temperature dependent and therefore can be taken to be independent of radial location. Inclusion of this temperature dependence would only contribute higher order effects in the solution and distract attention from the primary emphasis of examining the effects of rotation. Also, the only practical values for β are those less than or equal to one, as the fiber stiffness is always greater than the matrix (thereby resulting in $E_L \geq E_T$).

The general solution of this Euler-Cauchy governing equation is:

$$\sigma_r = C_1 r^{m_1} + C_2 r^{m_2} + Q_1(r) - Q_2(r) \tag{11}$$

where

$$Q_1(r) = \frac{r^{m_1}}{m_1 - m_2} \int r^{-(m_1+1)} Q(r) dr$$

$$Q_2(r) = \frac{r^{m_2}}{m_1 - m_2} \int r^{-(m_2+1)} Q(r) dr \tag{12}$$

$$m_1 = -1 + \Sigma, \qquad m_2 = -1 - \Sigma \quad \text{and} \quad \Sigma = \sqrt{\frac{1}{\beta}}$$

and C_1 and C_2 are constants to be determined from the applied mechanical boundary conditions.

The general solution for the tangential stress is obtained by merely substituting equation (11) back into (2):

$$\sigma_\theta = C_1(m_1+1)r^{m_1} + C_2(m_2+1)r^{m_2} + (m_1+1)Q_1(r) - (m_2+1)Q_2(r) + \rho\omega^2 r^2 \tag{13}$$

Whereupon, the radial deflection is derived by substituting equations (11) and (13) into (7) and the resulting expression into equation (5):

$$u_r = r\left[\frac{\sigma_\theta}{E_L} - \frac{v_L \cdot \sigma_r}{E_L} + \alpha_L\left(T_a - T_o + \frac{T_b - T_a}{b - a}(r - a)\right)\right] \tag{14}$$

To obtain the constants C_1 and C_2 appearing in equations (11) and (13), we impose the following boundary conditions along the inner and outer radius of the disk, i.e.,

$$(\sigma_r)_{r=a} = -P_{in}$$

$$(\sigma_r)_{r=b} = -P_{out}$$

where P_{in} and P_{out} are the internal and external pressures, respectively. Solving the resulting 2×2 matrix equation results in the following expressions:

$$C_1 = \frac{a^{1+\sqrt{\frac{1}{\beta}}}(P_{in} + Q_2(a) - Q_1(a)) - b^{1+\sqrt{\frac{1}{\beta}}}(P_{out} + Q_2(b) - Q_1(b))}{a^{2\sqrt{\frac{1}{\beta}}} - b^{2\sqrt{\frac{1}{\beta}}}} \tag{15}$$

and

$$C_2 = \frac{a^{\sqrt{\frac{1}{\beta}}}b^{\sqrt{\frac{1}{\beta}}}\left[-ab^{\sqrt{\frac{1}{\beta}}}(P_{in} + Q_2(a) - Q_1(a)) + ba^{\sqrt{\frac{1}{\beta}}}(P_{out} + Q_2(b) - Q_1(b))\right]}{a^{2\sqrt{\frac{1}{\beta}}} - b^{2\sqrt{\frac{1}{\beta}}}} \tag{16}$$

where we may separate the thermal and rotational terms such that

$$Q_1(r) = Q_1^T(r) + Q_1^R(r) \quad \text{and} \quad Q_2(r) = Q_2^T(r) + Q_2^R(r) \tag{17}$$

with the generalized thermal forces being defined as,

$$Q_1^T(r) = \frac{1}{2\sqrt{\frac{1}{\beta}}} \left(E_L(\alpha_L - \alpha_T) \frac{a(T_b - T_o) + b(-T_a + T_o)}{\left(-1 + \sqrt{\frac{1}{\beta}}\right)(a-b)} + \frac{rE_L(T_a - T_b)(2\alpha_L - \alpha_T)}{\left(-2 + \sqrt{\frac{1}{\beta}}\right)(a-b)} \right)$$

(18)

$$Q_2^T(r) = \frac{1}{2\sqrt{\frac{1}{\beta}}} \left(E_L(\alpha_L - \alpha_T) \frac{a(T_b - T_o) + b(-T_a + T_o)}{\left(-1 - \sqrt{\frac{1}{\beta}}\right)(a-b)} + \frac{rE_L(T_a - T_b)(2\alpha_L - \alpha_T)}{\left(-2 - \sqrt{\frac{1}{\beta}}\right)(a-b)} \right)$$

and those due to rotation as,

$$Q_1^R(r) = \frac{r^2 \rho \omega^2 (3 + \nu_L)}{2\sqrt{\frac{1}{\beta}}\left[-3 + \sqrt{\frac{1}{\beta}}\right]} \quad \text{and} \quad Q_2^R(r) = \frac{r^2 \rho \omega^2 (3 + \nu_L)}{2\sqrt{\frac{1}{\beta}}\left[-3 - \sqrt{\frac{1}{\beta}}\right]}$$

(19)

2.1.2 Solid Disk.—For the special case of a solid disk, the radial stress must remain finite at the center of the disk, therefore given either an *isotropic or anisotropic* material, it can be immediately seen that C_2 in equation (11) must be equal to zero (thus both displacement and stress fields at the center will be finite), such that,

$$\sigma_r = C_1 + Q_1(r) - Q_2(r)$$

(20)

for the isotropic case, and

$$\sigma_r = C_1 r^{m_1} + Q_1(r) - Q_2(r)$$

(21)

for the anisotropic case. Now assuming that an applied external pressure P_{out} exist, the constant C_1 is determined to be:

$$C_1 = P_{out} + Q_2(b) - Q_1(b)$$

(22)

for the isotropic case, or

$$C_1 = \frac{1}{r^{m_1}}[P_{out} + Q_2(b) - Q_1(b)]$$

(23)

for the anisotropic case. Where in the definitions for Q_1^T, Q_1^R and Q_2^T, Q_2^R given above in equations (18) and (19), a (the inner radius) is taken to be zero. Similarly, the tangential stress is

$$\sigma_\theta = C_1 + Q_1(r) + Q_2(r) + \rho\omega^2 r^2$$

(24)

for the isotropic case, and

$$\sigma_\theta = (m_1 + 1)C_1 r^{m_1} + (m_1 + 1)Q_1(r) - (m_2 + 1)Q_2(r) + \rho\omega^2 r^2$$

(25)

for the anisotropic case. Note, for the isotropic case, Q_1 and Q_2, can be greatly simplified by taking $\beta = 1$, with the resulting expressions being given in equation (29), see section 2.4.1.

2.2 Multiple Number of Concentric Disks

Extension of the formulation to "n" number of annular concentric disks, with possible misfit (see fig. 2), is simply accomplished through application of appropriate boundary conditions at the interface of each disks, so as to ensure continuity of radial stresses and displacements. Continuity of radial stress demands the following:

$$
\begin{aligned}
\sigma_{r_1}(r = r_1) &= P_1 \\
\sigma_{r_1}(r = r_2) &= \sigma_{r_2}(r = r_2) = P_2 \\
\sigma_{r_2}(r = r_3) &= \sigma_{r_3}(r = r_3) = P_3 \\
&\vdots \\
\sigma_{r_{n-1}}(r = r_n) &= \sigma_{r_n}(r = r_n) = P_n \\
\sigma_{r_n}(r = r_{n+1}) &= P_{n+1}
\end{aligned}
\tag{26}
$$

where P_1 and P_{n+1} are the applied internal and external pressures, respectively; whereas the remaining continuity conditions in (26) will then lead to the determination of the remaining interfacial pressures $P_2, P_3 ... P_n$ (which are redundant unknowns, for the common case of imposed (known) interference fit). Similarly, kinematic constraints are introduce at the interfaces corresponding to the imposed misfit (δ) at each interface. These are:

$$
\begin{aligned}
u_{r_2}(r = r_2) - u_{r_1}(r = r_2) &= \delta_1 \\
u_{r_3}(r = r_3) - u_{r_2}(r = r_3) &= \delta_2 \\
u_{r_4}(r = r_4) - u_{r_3}(r = r_4) &= \delta_3 \\
&\vdots \\
u_{r_n}(r = r_n) - u_{r_{n-1}}(r = r_n) &= \delta_{n-1}
\end{aligned}
\tag{27}
$$

Where $\delta_1, \delta_2, ...\delta_{n-1}$ are the imposed misfits between disks that will in turn generate interface pressures. Combining equations (26) and (27) with equations (11) and (14) specifies a system of $2n$ equations with $2n$ number of unknown constants; i.e.:

$$
[K]\{C\} = \{R\}
\tag{28}
$$

where

$\{C\}$ is the vector of unknown constants; $\{C\} = \left\{ C_1^1, C_2^1, C_1^2, C_2^2, \cdots, C_1^n, C_2^n \right\}^T$

$[K]$ is the geometry and material matrix

$[R]$ is the vector of applied forces and/or misfit parameters

2.3 Verification of the Solution

As indicated in the introduction, the analysis of isotropic and anisotropic disks subjected to rotation, internal and external pressure, temperature variation and misfit are not new (refs. 1 to 4). Consequently, the present unified solution can be, and has been, validated through comparison with a variety of other solutions, see table V for a brief summary. Clearly all aspects of the solution have been verified with at least one other independent numerical or analytical solution. In all cases the present solution agrees identically with all other analytical solutions and for all practical purposes identically with all FEA results as well. Figures 3 to 5 illustrate three of the many comparisons made between the present formulation results and other previous analytical results. In figure 3 the thermal and internal/external pressure analysis is compared against a previous analytical solution derived by Arnold (ref. 175), with the agreement being excellent. In figure 4 the analysis of an anisotropic disk subjected to pure rotation is compared

with Lekhnitskii's solution (ref. 58), again the agreement is excellent. Another example demonstrates the ability to include misfit within the formulation, see figure 5. Here comparison with Ugural and Fenster's (ref. 176) solution of two isotropic disks subjected to a misfit of 0.1 mm is made. The calculated contact pressure is, 12.305 MPa, while the tangential stresses in the outer and inner cylinder are:

$$\sigma_\theta(r = 200 \text{ mm}) = 56.055 \text{ MPa}$$
$$\sigma_\theta(r = 250 \text{ mm}) = 43.750 \text{ MPa}$$

and

$$\sigma_\theta(r = 150 \text{ mm}) = -56.250 \text{ MPa}$$
$$\sigma_\theta(r = 200 \text{ mm}) = -43.945 \text{ MPa}$$

respectively. These values agree exactly with those calculated by Ugural and Fenster (ref. 176)

2.4 Observations Regarding The Analytical Solution

Before conducting a parametric study to identify the important parameters in the design of flywheel systems, let us make a number of observations regarding the current analytical approach for conducting stress analysis by examining a number of special cases.

2.4.1 Material Isotropy.—For the special case of material isotropy (i.e., $\beta = 1$), the character of the governing equation (see eq. (9)) will change as the zeroth order term will disappear and consequently, the particular solution, i.e., equation (12), will be appropriately modified. The resulting expressions for Q_1 and Q_2 coming from equation (12) and including both thermal and rotational loading are:

$$Q_1(r) = r\left(\frac{E(T_a - T_b)\alpha}{2(a-b)} + \frac{r\rho\omega^2(3+v)}{-4} \right) \tag{29}$$

$$Q_2(r) = r\left(\frac{E(T_a - T_b)\alpha}{-6(a-b)} + \frac{r\rho\omega^2(3+v)}{-8} \right)$$

2.4.1 Thermal Isotropy.—Here let us consider the case when only thermal loading is applied to the disk. Under this condition it is apparent from equations (10) to (19) that, in general, the stress distribution (tangential and radial) is dependent upon geometry, material properties (i.e., strength of anisotropy), mismatch in thermal expansion coefficients, and the magnitude of the thermal load itself. In the case of thermal isotropy (i.e., when the tangential (α_L) and radial (α_T) thermal coefficients are equal) the stress distribution is primarily dependent only on β (the ratio of moduli) and E_L, as the constants C_1 and C_2 become a function of $Q_2 - Q_1$, that is:

$$Q_2 - Q_1 = \frac{rE_L(T_a - T_b)\alpha}{(a-b)(4 - \frac{1}{\beta})} \tag{30}$$

Consequently, under a uniform temperature distribution no stresses are developed as one might expect. Also in general, from equations (10) and (14), it is apparent that the longitudinal thermal coefficient is the dominant parameter with the longitudinal modulus dictating the magnitude of thermal stresses being developed.

2.4.2 Numerical Singularities.—It is well know that nonphysical numerical singularities can exist within an analytical solution, and these vary depending upon the approach taken. In the above derivation the final governing equation to be solved is stress based, therefore we will examine the resulting radial stress under various special conditions so as to identify all potential singularities. As the solution is limited to elastic behavior the concept of superposition applies; consequently individual-loading conditions can be examined separately. This will greatly simplify the current task. The following four possible loading cases (rotation, pressure, thermal and interfacial misfit) were taken under consideration.

Rotation Only: Given a single, annular, disk subject to only rotation, the radial stress equation (11) becomes:

$$\sigma_r = \frac{(3+v_L)\rho\omega^2}{\frac{1}{\beta}-9}\left\{\left[\frac{\left(b^{\left(3+\sqrt{\frac{1}{\beta}}\right)}-a^{\left(3+\sqrt{\frac{1}{\beta}}\right)}\right)}{\left(a^{2\sqrt{\frac{1}{\beta}}}-b^{2\sqrt{\frac{1}{\beta}}}\right)}r^{\left(-1+\sqrt{\frac{1}{\beta}}\right)}-\frac{a^{\sqrt{\frac{1}{\beta}}}b^{\sqrt{\frac{1}{\beta}}}\left(b^3a^{\sqrt{\frac{1}{\beta}}}-a^3b^{\sqrt{\frac{1}{\beta}}}\right)}{\left(a^{2\sqrt{\frac{1}{\beta}}}-b^{2\sqrt{\frac{1}{\beta}}}\right)}r^{-\left(1+\sqrt{\frac{1}{\beta}}\right)}+r^2\right]\right\} \tag{31}$$

Clearly, a singularity would exist in the solution whenever β approaches $1/9$ (i.e., whenever $E_L = 9E_T$). This type of singularity has been found before in other solutions, such as Lekhnitskii (ref. 58) and more recently for the case of solid disks, as discussed in reference 177, for values of $\beta > 1$. Once again confirming the accuracy of the present formulation.

Pressure Only: Solving for the single, annular, disk case subjected to both inner and outer pressure (P_{in} and P_{out}, respectively), the following equation for the radial stress can be derived:

$$\sigma_r = \frac{r^{-1-\sqrt{\frac{1}{\beta}}}\left\{a^{\sqrt{\frac{1}{\beta}}}b^{\sqrt{\frac{1}{\beta}}}\left(-ab^{\sqrt{\frac{1}{\beta}}}P_{in}+ba^{\sqrt{\frac{1}{\beta}}}P_{out}\right)+r^{2\sqrt{\frac{1}{\beta}}}\left(a^{1+\sqrt{\frac{1}{\beta}}}P_{in}+b^{1+\sqrt{\frac{1}{\beta}}}P_{out}\right)\right\}}{\left(a^{2\sqrt{\frac{1}{\beta}}}-b^{2\sqrt{\frac{1}{\beta}}}\right)} \tag{32}$$

For any finite disk, a can not equal b in equation (32), and consequently there is no possible singularity for this type of loading.

Thermal Loading Only: Again considering a single, annular disk, subjected to a pure thermal loading condition, the derived expression for the radial stress becomes somewhat lengthy; consequently, for convenience, only the denominator (which would be the source of any numerical problem) of the troublesome term will be shown here.

$$\sigma_r = \frac{Numerator}{\frac{1}{\beta}(a-b)\left(a^{2\sqrt{\frac{1}{\beta}}}-b^{2\sqrt{\frac{1}{\beta}}}\right)(\beta-1)(4\beta-1)} \tag{33}$$

Clearly the solution has two singularities, namely whenever $\beta = 1/4$ (i.e., $E_L = 4E_T$) or $\beta = 1$ (i.e., $E_L = E_T$, which is the isotropic case).

Misfit only: The simplest problem containing a misfit is that of two disks with a misfit, δ, imposed between the inner and outer disks, see figure 6, where a and b are the inner and outer radii, respectively and c designates the radial location of the misfit. Solving for the radial stress in both the inner and outer disks, respectively, we get the following expressions:

Inner disk

$$\sigma_r = \frac{E_L \, r^{-1-\sqrt{\frac{1}{\beta}}} \, c^{-\sqrt{\frac{1}{\beta}}}\left(b^{2\sqrt{\frac{1}{\beta}}} - c^{2\sqrt{\frac{1}{\beta}}}\right)\left(a^{2\sqrt{\frac{1}{\beta}}} - r^{2\sqrt{\frac{1}{\beta}}}\right)\delta}{2\sqrt{\frac{1}{\beta}}\left(b^{2\sqrt{\frac{1}{\beta}}} - a^{2\sqrt{\frac{1}{\beta}}}\right)} \tag{34}$$

Outer disk

$$\sigma_r = \frac{E_L \, r^{-1-\sqrt{\frac{1}{\beta}}} \, c^{-\sqrt{\frac{1}{\beta}}}\left(a^{2\sqrt{\frac{1}{\beta}}} - c^{2\sqrt{\frac{1}{\beta}}}\right)\left(b^{2\sqrt{\frac{1}{\beta}}} - r^{2\sqrt{\frac{1}{\beta}}}\right)\delta}{2\sqrt{\frac{1}{\beta}}\left(b^{2\sqrt{\frac{1}{\beta}}} - a^{2\sqrt{\frac{1}{\beta}}}\right)} \tag{35}$$

It is obvious from examining equations (34) and (35) that for the case of misfit only, no singularities exist over the domain.

Given the results of the above four loading cases it is apparent that a pattern has emerged, thus prompting a generalization regarding the potential for the existence of numerical singularities. One can expect singularities to be present whenever body forces are imposed upon a given solution; however, when the excitation is arising due to the application of imposed boundary conditions (i.e., applied tractions or displacements) no singularities should be expected to occur.

3.0 INFLUENCE OF KEY DESIGN PARAMETERS

Having developed and verified a general analytical solution for multiple, anisotropic, concentric disks, with misfit, subjected to rotation, pressure and thermal loading, we are now in a position to identify and examine the influence of important design parameters such as: mean radius, thickness, the amount of misfit, rotational speed, and material gradation. Two classes of anisotropic (composite) materials are primarily employed throughout this study. The first class, polymeric matrix composite (PMCs) systems, is represented by a 60 vol % fraction graphite/epoxy system. The second class, titanium matrix composite (TMCs) systems, is represented by a 35 vol % fraction SiC/Ti-15-3. Subsequent to examining a single disk composed of a uniform volume fraction of material, examination of material gradation and misfit effects will be undertaken by considering three concentric disks with varying fiber volume fractions.

Flywheels composed of PMC material systems are currently being investigated under the NASA funded Rotor-Safe-Life Program (RSL); a collaborative government/industry program designed to establish a certification procedure for composite flywheels. Consequently, this material class will dominate the parametric study. The associated material properties for the two classes of composite systems (and their individual fiber and matrix constituents) used in this study are listed in tables VI and VII, where the composite properties were obtained using the micromechanics analysis code based on the generalized method of cell, MAC/GMC (ref. 178). All properties given are at room temperature and assumed to be independent of temperature. The flywheels to be considered in the RSL program are expected to have a mean radius of approximately 4 in. and a thickness of approximately 3 in.; therefore these geometric properties will constitute our baseline case.

Considering the case of a single annular disk, subjected to pure rotation, the influence of the three key material and geometric parameters (i.e., the degree of material anisotropy (β), mean radius (R_m) and thickness $(\beta \therefore \lambda)$) on the radial and tangential stress distribution will be investigated parametrically. Analytically, these parameters can be clearly seen by normalizing both the radial (see eq. (31)) and tangential stress (see eq. (2)) with respect to the density, rotational speed, and outer radius, b, that is:

$$g(\beta, R_m, \lambda, \nu_L) = \frac{\sigma_r}{\rho\omega^2 b^2} = \frac{(3+\nu_L)}{\frac{1}{\beta}-9}\left\{\frac{\left(1-\left(\frac{a}{b}\right)^{\left(3+\sqrt{\frac{1}{\beta}}\right)}\right)}{\left(\left(\frac{a}{b}\right)^{2\sqrt{\frac{1}{\beta}}}-1\right)}\left(\frac{r}{b}\right)^{\left(-1+\sqrt{\frac{1}{\beta}}\right)} - \frac{\left(\left(\frac{a}{b}\right)^{\sqrt{\frac{1}{\beta}}}-\left(\frac{a}{b}\right)^3\right)}{\left(\left(\frac{a}{b}\right)^{2\sqrt{\frac{1}{\beta}}}-1\right)}\left(\frac{a}{b}\right)^{\sqrt{\frac{1}{\beta}}}\left(\frac{b}{r}\right)^{\left(1+\sqrt{\frac{1}{\beta}}\right)} - \left(\frac{r}{b}\right)^2\right\}$$

(36)

$$f(\beta, R_m, \lambda, \nu_L) = \frac{\sigma_\theta}{\rho\omega^2 b^2} = \frac{(3+\nu_L)}{\frac{1}{\beta}-9}\left\{\sqrt{\frac{1}{\beta}}\frac{\left(1-\left(\frac{a}{b}\right)^{\left(3+\sqrt{\frac{1}{\beta}}\right)}\right)}{\left(\left(\frac{a}{b}\right)^{2\sqrt{\frac{1}{\beta}}}-1\right)}\left(\frac{r}{b}\right)^{\left(-1+\sqrt{\frac{1}{\beta}}\right)}\right.$$

$$\left. + \sqrt{\frac{1}{\beta}}\frac{\left(\left(\frac{a}{b}\right)^{\sqrt{\frac{1}{\beta}}}-\left(\frac{a}{b}\right)^3\right)}{\left(\left(\frac{a}{b}\right)^{2\sqrt{\frac{1}{\beta}}}-1\right)}\left(\frac{a}{b}\right)^{\sqrt{\frac{1}{\beta}}}\left(\frac{b}{r}\right)^{\left(1+\sqrt{\frac{1}{\beta}}\right)} + \left(\frac{\frac{1}{\beta}+3\nu_L}{3+\nu_L}\right)\left(\frac{r}{b}\right)^2\right\}$$

(37)

where the inner and outer radii are defined as

$$a = R_m - \frac{\lambda}{2}$$
$$b = R_m + \frac{\lambda}{2}$$
$$\text{and} \quad \frac{a}{b} = \frac{1-\frac{\lambda}{2R_m}}{1+\frac{\lambda}{2R_m}}$$

so that $g(\beta, R_m, \lambda, \nu_L)$ and $f(\beta, R_m, \lambda, \nu_L)$ will be denoted as the radial and tangential distribution factors, respectively, for an anisotropic annular disk.

Figures 7 and 8 depict these factors as a function of normalized radial location, r/R_m, for two limiting geometric representations, i.e., a thick disk $(\lambda/R_m \approx 2.0)$ and a thin disk $(\lambda/R_m \approx 0.125)$, given a slightly anisotropic $(\beta = 0.7)$ TMC, and strongly anisotropic $(\beta = 0.05)$ PMC material description, respectively. Further, in table VIII the maximum values of the modified normalized radial and tangential stress are given for a range of thickness and mean radii. From these results one can draw a number of conclusions.

The first being that both the radial and tangential stresses increase as R_m and λ are increased (see table VIII). The second is that the degree of material anisotropy (β) impacts the magnitude of increase in the radial stress component more so than the tangential stress component, and this influence increases as the thickness is increased; whereas, it diminishes as the mean radius is increased. In fact, once the disk is sufficiently "thin," i.e., $\lambda/R_m < 0.125$, the degree of material anisotropy becomes irrelevant. Thirdly, the location of the maximum stress is also greatly impacted by the degree of anisotropy. For example in figure 7, we see that for the strongly anisotropic PMC material system the maximum tangential stress location varies greatly depending upon mean radius; whereas for the slightly anisotropic TMC material system, see figure 8, the maximum tangential stress is always at the inner radius. Similarly, the location of the maximum radial stress shifts from approximately $0.75 R_m$ to R_m as the mean radius increases for a TMC (see fig. 8). Whereas for a PMC (see fig. 7) material the maximum location moves from $1.25 R_m$, for small mean radii, towards the center (i.e., R_m) as the mean radius, R_m, is increased. These observations were substantiated by the work of Gabrys and Bakis (ref. 179) wherein they designed and tested a flywheel that employed a much softer urethane matrix, which precluded the development of a large radial stress. This then allowed the use of thick flywheels, wherein the maximum hoop stress was shifted so that it occur near the OD; thereby theoretically leading to a less catastrophic failure mode and fail-safe flywheel design. Fourthly, irrespective of the degree of material anisotropy the most efficient use of material is made when one considers the case of relatively thin disks rather than thick ones, see figures 7 and 8. This will be discussed further in the subsequent material and configuration selection section. Finally, it is obvious from equations (36) and (37) that the density (ρ) of the material impacts the actual magnitude of the stress field (both radial and tangential components) linearly, while the rotational speed (ω) impacts both components quadratically.

The radial and tangential stress distributions as a function of normalized radial location for pure thermal loading and internal pressure loading are shown in figures 9 and 10; assuming the baseline material parameters corresponding to the 60 vol % fraction PMC system in table VI for a relatively thick disk ($R_m = 4$ in. and $\lambda = 3$ in.). From figure 9, we see that temperature (whether uniform or gradient) induces compressive hoop stress in the outer portion of disk and tensile hoop stress in the inner portion. However, in the presence of a linearly varying temperature field, the slope (positive or negative) of the gradient of temperature will shift the maximum location of the tensile radial stress from one side of the disk to the other, as well as change the curvature of the hoop stress distribution and the magnitude of the maximum tensile hoop stress.

In figure 10 the influence of applying pressure along the inner surface of the disk is illustrated. This type of loading distribution would be consistent with the presence of a solid hub (shaft), albeit in practice it is clear that the magnitude of this internal pressure would be a function of the density, size and speed of rotation of this solid hub. Consequently, in figure 10 both the radial and tangential stress profiles are normalized with respect to the applied internal pressure. The basic influence of internal pressure is to induce a compressive radial stress state and tensile hoop stress throughout the annular disk, with a maximum in both stress components occurring at the inner radius. Further, discussions regarding the influence of internal/external pressure and temperature profiles for single cylindrical or disk configurations can be found in reference 175.

Now the superposition of these three classes of loads (thermal, internal pressure, and rotation) is illustrated in figures 11 and 12; where both radial and hoop distributions are shown for a relatively thick disk ($\lambda = 3$, $R_m = 4$) rotating at 15 000 rpm (fig. 11) and 60 000 rpm (fig. 12) subjected to both uniform and gradient temperature profiles and an internal pressure of 1 ksi. Note how for the lower speed case (fig. 11), the overall conclusions for the combined loading situation are similar to those of the pure thermal cases; with the exception of tensile hoop stress being present even in the outer region of the disk for both the uniform and inner gradient case. Tensile hoop stresses are present in these two cases because the tensile hoop stress generated, due to rotation, are sufficiently high to overcome the thermally induced compressive hoop stresses in the outer region. In addition we see immediately that at the inner radius the radial stress becomes compressive due to the applied internal pressure, while it is zero at the outer surface, as it must be. Figure 12 clearly shows that as the rotational speed is increased to 60 000 rpm the stresses due to rotation dominate those induced by either the internally applied pressure or the imposed thermal profiles. Note, however, that the hoop stress distribution becomes almost uniform across the disk, thus making more efficient use of the material.

3.2 Three Concentric Disks

In the RSL program the flywheels of interest are being manufactured with a preload design in mind, that is the flywheel is composed of a number of concentric rings press-fit together with a specified misfit between each ring. Therefore, the resulting laminated flywheel has a compressive radial stress at the interface of each concentric ring. Consequently, the desire here is to investigate the influence of a key design parameter (i.e., misfit, δ between disks) on the corresponding radial and tangential stress distribution within the laminated system. This parameter is in addition to the two previous geometric parameters: R_m – mean radius and λ – ring thickness in the radial direction. When examining the influence of δ, tracking of the radial stress distribution is important, since a positive value at a given interface will constitute (by definition) disk separation. Similarly, if the radial stress exceeds some critical value, delamination within a given disk may also take place. Alternatively, the tangential (or hoop) stress is significant in that it will dictate the burst failure of a given ring (disk) within the system, which may or may not (depending upon the location) lead to an immediate catastrophic failure of the entire system. The limit speed of a given, circumferentially reinforced, disk is dictated by the circumferential (or hoop) stress, thus excessive hoop stress will result in fiber breakage and a subsequent total loss in load carry ability. Consequently, this failure criterion is defined as the burst criterion.

3.2.1 Uniform Material Properties.—To simplify the study, only three (each with the 60 vol % fraction PMC system given in table VI) concentric disks will be investigated with a baseline geometry similar to the previous single disk case, that is, an $R_m = 4$ and a total thickness (i.e., $\lambda_1 + \lambda_2 + \lambda_3$) equal to 3 in. A three disk minimum is required so that the influence of two misfits can be examined, that is the misfit between disk 1 and disk 2, δ_1, and that between disk 2 and disk 3, δ_2, see figure 13. When considering applying a misfit at an interface one could specify a similar misfit directly for each interface or alternatively specify a given mismatch in hoop strain for all interfaces. The first option would effectively result in applying different amounts of hoop strain at each interface, whereas, the second option would result in different misfits being specified for each interface. In an attempt to isolate the interaction of mean radius and misfit, the constant applied hoop strain approach to selecting the appropriate misfit at each interface is taken. Consequently, each displacement misfit applied is proportional to the radial location of the corresponding interface (i.e., $\delta_i = \varepsilon_h R_i$) such that a constant hoop strain (ε_h) at each interface is imposed. In this way the impact of the misfit will be consistently felt even when the mean radius is increased.

Assuming only rotational loading with a speed (ω) of 30 000 rpm, analysis results for the disk system are shown in figures 14 and 15, when the overall mean radius and misfit hoop strain are varied as follows: $R_m = 2, 4,$ and 6 in. and $\varepsilon_h = 0., 0.1$ and 0.2 percent. In figures 14 and 15, the radial stress versus radial location and tangential stress versus radial location are shown respectively, for each of the above cases. Examining figure 14 it is apparent that in the case of no misfit ($\varepsilon_h = 0$, see fig. 14(a)) all radial stresses are tensile. Recalling from figures 11 and 12, it is clear that even if internal pressure was applied to offset these rotationally induced stresses only the inner most surface would experience compressive radial stress, while the remainder of the disk would remain in a state of tension. The extent of the compressive region is dependent upon (as shown in fig. 10) the magnitude of the imposed inner pressure. However, increasing this inner pressure (e.g., in the case of a mass loaded design) is of only limited value as this compressive region rapidly becomes tensile as one proceeds toward the outer diameter of the disk system.

Alternatively, if one imposes a prestress through application of a misfit at the interfaces between disks, a compressive radial stress state can be induced throughout. These interfacial compressive radial stresses (denoted in figures 14(b) and (c) by an I_1 and I_2) then increase as the misfit hoop strain is increased for a given mean radius. Note that even though the imposed hoop strain mismatch is the same at all interfaces, within the system, the first interface, I_1, is more compressive as it benefits from the compressive state at I_2 as well. Furthermore, figure 14 clearly demonstrates that as the overall mean radius of the system is increased, the effectiveness of the imposed hoop strain is reduced; even to the extent of not inducing any compressive stresses.

Figure 15 illustrates the tangential stress distribution for various mean radii and magnitudes of hoop strain mismatch (misfit) between the disks. Examining figure 15, it is apparent that, (1) the location of the maximum tensile hoop stress (and thus the initiation of fiber breakage and failure) changes and (2) the magnitude of the hoop stress increases as the mean radius is increased, given a specified amount of hoop strain mismatch. In addition, in the presence of misfit, the tangential (hoop) stress profile is discontinuous and forms a stair step pattern, with each subsequent disk within a given system, typically having a higher stress state than the previous. Consequently, given an interfacial misfit and the given material anisotropy, one can be assured that failure would initiate at the inner radius of the outer most disk, provided the overall system is not relatively thin, i.e., $\lambda/R_m > 0.3$. Nevertheless, it is apparent

that a complex relationship between the various geometric parameters, δ, λ, and R_m exists (as suggested by eqs. (34) and (35) for the case of two disks).

Selecting a proper disk thickness configuration is another important aspect that was investigated. Figure 16 shows three arrangements with different individual disk thickness but all adding up to the same overall total thickness. Examining the figure it can be concluded that the most beneficial arrangement is that of two thinner inner rings surrounded by a thicker outer ring. As this arrangement provides a maximum compressive radial stress state while giving a lower maximum hoop stress within the outer ring. Clearly, the thicker outer ring could fail (as could all other configurations) by delamination due to excessive tensile radial stress. However, for this particular case delamination and burst would be confined to the outer ring, which should be a more fail-safe design than either of the other two configurations examined.

   3.2.2 Nonuniform Material Properties and/or Loads.—The goal of any design is to maximize the allowable rotational speed before either a disk separation (in a preload design) or burst criterion is exceeded. Although, in equations (34) and (35), both disks were assumed to be comprised of the same transversely isotropic material, it is apparent that not only is the magnitude of misfit important in the determination of the radial stress at the interface but so too are the material properties. Consequently, this led us to investigate the influence of gradation of the material properties within the laminated system. As a result, the six cases identified in table IX were examined. The first three cases being PMC (strongly anisotropic) laminated systems and the last three TMC (slightly anisotropic) systems. An additional motivation (besides the degree of anisotropy) behind investigating an idealized TMC system as well as a PMC system, is the ability to examine the trade-offs between density and stiffness/strength. Since in a PMC system, as the volume fraction of reinforcement is increased the density (weight) of the material as well as stiffness and strength also increase. Alternatively in a TMC as the fiber volume fraction is increased the density of the material is reduced, while the stiffness and strength are increased. Albeit, this later density consideration will be small and in practicality higher order when compared to the variation in stiffness and strength. Even so, the induced body forces due to rotation, and thus influence of gradation effects is different between the two classes of materials.

   Case one is identical to the baseline material examined thus far; consequently, case two through six will be subjected to the same conditions. These are a rotational speed (ω) of 30 000 rpm, variation of mean radius ($R_m = 2, 4,$ and 6 in.) and imposition of constant hoop strain (ε_h) at each interface of 0, 0.1 and 0.2 percent (i.e., variable misfit, δ, per interface such that $\delta_i = \varepsilon_h R_i$). Again the representative model TMC material properties are given in table VII. The results of these analyses are presented in figures 17 to 20, where the radial stress versus radial location and tangential stress versus radial location are shown, respectively, for all three cases.

   Examining these figures it is clear that material and density gradation play a major role in the resulting radial and tangential stress distributions; the geometric and strength of anisotropy effects being similar in nature to those discussed at length previously. In particular, note how the radial compressive stress at the disk interfaces can be increased or completely eliminated depending upon the imposed material gradient. Similarly, the magnitude of the stair steps in the tangential stress as well as the maximum value and location of this stress are also greatly impacted by gradation. For example, note the difference between case two and three (compare, figs. 18(b) and (c)) in that for case two burst failure would initiate in the outer ring, whereas in case three it would most likely initiate in the middle ring, all else being equal. A similar trend is observed for the TMC cases, wherein case 5 (fig. 20(b)) would initiate burst failure in the outer ring and case 6 (fig. 20(c)) clearly would initiate failure in the inner ring given sufficient rotational speed.

   Since cases 2 and 5 had the most favorable material gradient with respect to minimizing the potential for disk separation (i.e., maximizing the speed of rotation prior to disk separation) the influence of misfit and rotational speed will be examined given these configurations. The results are presented in figures 21 to 23. In figures 21 and 22 it is apparent that material gradation naturally leads to higher compressive (or at the least, smaller tensile) interfacial stress as the mean radius is increased until the ratio of thickness to mean radius becomes small and the influence saturates. Also, increasing the misfit (imposed hoop strain) leads as before to an increase in radial compressive stress. However, now since the outer disk is significantly stiffer than the inner disks, the compressive stress at interface I_2 is now greater than I_1. This result is in contrast to those given in figure 14. Further, for a fixed misfit strain, the radial stress generally increases with increasing mean radius; although this is dependent upon the magnitude of the mean radius. Given the previous discussion (see fig. 9) regarding temperature gradient results, one can envision that imposing an appropriate temperature gradient would lead to similar results as that of material gradation, since in essence the material properties as well as imposed internal thermal stresses will be nonuniform and naturally lead to increases in radial compressive stresses.

Finally, from figure 23, it can be clearly seen that increasing the rotational speed (ω), decreases the compressive stress at an interface (possibly eliminating it altogether depending upon the magnitude of mean radius, for a given misfit) as expected. One must keep in mind, that increasing the rotational speed significantly increases (proportional to ω^2) the hoop (tangential) stress thus leading to potential burst failure of the system. Once again, from a design point of view all of these important parameters (misfit, mean radius, speed, material properties, and gradients of properties and/or loads) must be simultaneously optimized to achieve the "best" design.

4.0 MATERIAL AND CONFIGURATION SELECTION

In the previous section we spent a significant amount of time understanding the key design parameters that influence a single (or system of) rotating disks; such as mean radius, thickness, misfit, speed, material properties, and gradients of properties and/or loads. The interrelationship among these various parameters can be quite complicated and therefore typically requires a rigorous analysis be performed for each configuration (material and/or geometry) investigated. In this study we have focused primarily on two classes of composite materials, PMC and TMC, given a range (from relatively thick to thin) sizes of annular disks. In this section we will confine ourselves to single (solid or annular) disk configurations with constant height and attempt to determine the best configuration for maximizing energy storage. Clearly, an efficient flywheel stores as much energy per unit weight as possible, without "failing". Failure can be defined in a number of different ways (e.g., uniaxial, multiaxial, burst criterion, or disk separation), induced as a result of several factors (e.g., over-speed (burst), decay of material properties (due to environmental factors), fatigue and/or creep conditions) and is dependent upon the specific application. Typically failure is dictated when the largest stress (i.e., hoop stress, see table VIII) due to centrifugal forces reaches the tensile strength (under burst conditions) or the fatigue strength (under cyclic conditions) of the material. The utilization, however, of anisotropic materials has made defining failure even more challenging as now the material strengths and properties are different in the various material directions and new modes of failure may be introduced.

The "best" flywheel system is one that maximizes the kinetic energy per unit mass without failure. In practice, it should be remembered that the mass considered should be that of the whole system and the energy stored should be assessed only as the energy that can be supplied in normal service. Here, however, we will concern ourselves with the kinetic energy of the spinning disk, only. Consequently, given that this energy is defined as, $U = J\omega^2/2$, with J being defined as the polar moment of inertia of the annular disk $J_{Annular} = \pi\rho t(b^4 - a^4)/2$, or solid (with $a = 0$, i.e., $J_{solid} = \pi\rho t b^4/2$) and the mass of the annular disk being $m_{Annular} = \pi\rho t(b^2 - a^2)$, or solid (with $a = 0$, such that $m_{solid} = \pi\rho t b^2$), one can obtain easily the following ratio, which needs to be optimized, that is:

$$\left(\frac{U}{m}\right)_{solid} = \omega^2\left(\frac{b^2}{4}\right) \tag{38}$$

or

$$\left(\frac{U}{m}\right)_{Annular} = \omega^2\left(\frac{b^2 + a^2}{4}\right) \tag{39}$$

depending upon the desired geometry.

To maximize the energy per unit mass, the task now becomes one of determining the maximum rotation speed (ω) that a given disk configuration (be it material and geometric) can withstand before the induced stresses (or strains) exceed some allowable limit. In the case of determining the limit (burst) speed of the disk one would use the ultimate tensile strength of the material; whereas in the case of fatigue (where the disk is spun up and down repeatedly) one would most likely use the endurance limit as the design allowable stress. Note, that in the case of anisotropic materials (e.g., PMCs and TMCs) these allowable limits will be significantly different depending upon orientation and fiber volume fraction. For example in the case of PMCs the ratio of longitudinal to transverse ultimate tensile strength is approximately 30 to 1, whereas in the case of TMCs this ratio is 3 to 1. This together with the fact that the induced stress field is biaxial, makes the identification of an appropriate multiaxial failure criteria very important.

To illustrate this fact we will examine three separate failure conditions to determine the maximum speed of rotation for both a solid and annular flywheel. The first two conditions, limit the speed based solely on a single (uniaxial) stress component (i.e., tangential (longitudinal direction) and radial (transverse direction) stress, respectively). Alternatively, the third is based on an equivalent transversely isotropic effective (J_2) stress measure (multi-axial) described more fully in the next section, see equation (59), as well as in references 185 and 188. Returning to equations (36) and (37) it can be shown that the maximum rotation speed is either

Hoop Stress Only

$$\omega^2_{max} \leq \left(\frac{\sigma_{u_L}}{\rho}\right) \frac{1}{b^2 f(a,b,\beta,r,\nu_L)} \tag{40}$$

or

Radial Stress Only

$$\omega^2_{max} \leq \left(\frac{\sigma_{u_T}}{\rho}\right) \frac{1}{b^2 g(a,b,\beta,r,\nu_L)} \tag{41}$$

or

Multiaxial Condition

$$\omega^2_{max} \leq \left(\frac{\sigma_{u_L}}{\rho}\right) \frac{1}{b^2 \sqrt{\left\{\xi^2 g^2 + f^2 - g \cdot f\right\}}} \tag{42}$$

where $\xi = \dfrac{\sigma_{u_L}}{\sigma_{u_T}}$

depending upon the desired failure condition utilized. The above expressions are quite general in that they can be used for both an annular $(a \neq 0)$ or solid $(a = 0)$ disk as well as a transversely isotropic $(\beta < 1)$ or isotropic material $(\beta = 1)$. Ashby (ref. 182) has derived a similar expression to that of equation (40) for the special case of a solid, isotropic disk. In (ref. 182) Ashby denoted the term σ_{u_L}/ρ as a performance index and employed it as a discriminator for the selection of the optimum material from which to construct a flywheel. The optimum material selected was a graphite (CFRP) or glass (GFRP) reinforced epoxy system, which can store between 150 to 350 KJ/kg of energy. It is interesting to note that the current work provides similar overall trends, however, the specific form now has an additional anisotropic factor that will modify the performance index suggested by Ashby (ref. 182) thereby making it more accurate. Inclusion of this additional factor requires that the appropriate anisotropic material properties be included in any database used to select between both monolithic (isotropic) and composite (anisotropic) materials.

In the past others (e.g., see refs. (1) and (2)) have expressed the performance index coming from the specific energy for isotropic systems as

$$\frac{U}{m} = \overline{K}\left(\frac{\sigma_{uL}}{\rho}\right) \tag{43}$$

where $\overline{K}$ was defined to be geometric shape factor. Furthermore, it was only noted in passing in the literature that this shape factor will become significantly more complex in the presence of anisotropic material behavior. Now by combining equations (39) and (42) one can define this complex "shape" factor, which accounts for both material anisotropy and stress state multiaxiality to be:

$$\overline{K} = \frac{1}{\sqrt{\left\{\xi^2 g^2 + f^2 - g \cdot f\right\}}}\left(\frac{b^2 + a^2}{4b^2}\right) \tag{44}$$

Clearly this shape factor (only valid as shown here for constant height disks) is no longer just a geometric parameter but in actuality has both material and geometric attributes, $\overline{K} = \overline{K}(\beta, \xi, a/b, \nu_L)$ such that now both $\overline{K}$ and σ_{u_L}/ρ become integral to the performance index.

Invoking the corresponding maximum speed resulting from the three criteria; the calculated stored kinetic energy per unit mass (specific energy), given an annular and solid disk made of the three PMC and TMC materials defined in tables VI and VII, are given in tables X and XI, respectively. Examining the results a number of conclusions become obvious. First, as expected from equations (38) and (40) to (42), the specific energy within a solid disk is independent of its geometry and only influenced by the degree of material anisotropy (stiffness and strength (UTS)). Secondly, for given annular disk, the specific energy increases as the mean radius is increased. This conclusion is particularly apparent when using the multiaxial criterion. Alternatively, however, the hoop only criterion does not show such a clear monotonic increase with increasing mean radius (as the location of the maximum hoop stress moves, this is particularly true for the case of strong anisotropy and relatively thick disks, see figs. 7 and 8), thus demonstrating the advantage of using a multiaxial criterion. Thirdly, it is apparent that the multiaxial criterion naturally accounts for the geometry of the disk; in that if a relatively thick anisotropic (with a weak bond between fiber and matrix) disk is analyzed the controlling stress is the radial component, whereas in the case of a relatively thin disk the hoop stress dominates. From tables X and XI it is apparent that the analyst would need to appreciate and account for this fact if they restricted themselves to using a simple uniaxial criterion. Fourthly, annular anisotropic disks are more efficient than solid anisotropic disks, see table XII. This is in sharp contrast to the fact that for isotropic materials, the specific energy of a solid disk is somewhere between 20 percent (for a thin annular disk) to 100 percent (for a thick annular disk) more efficient than its annular counterpart. Note also, that if one where to only utilizes the hoop stress criterion, one would incorrectly conclude that in the case of only slightly anisotropic materials (TMCs) a solid disk is more efficient than an annular disk. Once again demonstrating the importance of using a multiaxial criterion in the presence of a multiaxial stress field.

Finally, if we examine the ratio of the specific energy of PMC flywheels to that of TMC flywheels, it is apparent that flywheels made from PMCs are at least comparable to those made with TMCs, and more often they are approximately three times better (particularly for large sized flywheels (see table 13)). This result is not unexpected as PMCs are typically 2.5 times lighter than TMCs and as suggested by the above performance index, density plays a significant role. Also, as noted in table XIII the manufacturable fiber volume fraction of PMCs are typically significantly higher than TMCs and consequently the ultimate longitudinal strength of PMCs are typically significantly greater (1.5) than that of TMCs (compare tables XI and XII). However, the transverse strength of PMCs are approximately 0.2 that of TMCs; thus explaining why if one were to employ only a radial failure criterion, PMC flywheels would only perform approximately 0.3 to 0.5 as well as TMC flywheels, see table XIII. Remember however, that thus far only a static failure condition (ultimate tensile strength) at room temperature has been used to determine the maximum allowable rotational speed; which is key to calculating the maximum stored energy. Under fatigue conditions and/or at elevated temperatures TMC flywheels may out perform flywheels made of PMCs. This will be a topic of future study.

5.0 FAILURE ANALYSIS

A key factor in any design is the ultimate load capacity of a given structure. Flywheels are no exception. The desire here is to maximize the energy storage per unit mass without experiencing catastrophic failure of the system. Again, for simplicity we will limit our discussion to that of a single rotating annular disk of constant height and examine the allowable limit speed under both monotonic and cyclic load histories. Multiple disk configurations with imposed misfit will be addressed in the future.

5.1 Burst (Rupture) Limit

As mentioned previously, numerous failure criterions can be defined, e.g., disk separation, delamination within a disk, or a burst criterion. Here our concern will be with calculating the burst pressure or burst speed of a single annular disk. Although, within the current RSL program disk separation is the primary design consideration, burst conditions must still be established. Currently, hydroburst tests are being considered as potential certification tests for establishing the quality of the flywheel configurations being manufactured. However, one should always remember that for a general flywheel configuration the character of the problem changes significantly when going between internal pressure (hydroburst test) and rotation (spin test). That is, under internal pressure the ordering of the stresses is such that σ_r is always minimum (compressive), σ_z the intermediate and σ_θ the maximum (tensile) value; whereas,

under rotation all stresses are tensile, with σ_r being either an intermediate value, in the case of plane stress, or a minimum in the case of plane strain. This stress state may be altered depending upon the design selected (e.g., a preloaded multidisk design will have compressive radial stress component throughout provided the preload is sufficient). Therefore, although spin tests are considerably more expensive than their hydroburst counterparts, they still remain the most prototypical and representative tests and thus the ultimate certification tests. Consequently, we are also interested in calculating the limit (burst) speed for a given rotating flywheel configuration.

5.1.1 First Fracture.—An approach to calculating the burst limit for a circumferentially reinforced disk, for either internal pressure or rotation, is to define burst failure to be at the instant that the maximum hoop stress exceeds the material's ultimate tensile strength in the fiber direction (longitudinal). However, as we showed in the previous section, a more consistent criterion (than just the hoop stress alone) is to utilize an equivalent transversely isotropic effective stress (multiaxial) criterion. Consequently, the limit pressure and limit speed based on first fracture (at the location of maximum effective stress) are:

$$(P_{in})_{\text{limit}} = \left(\frac{\sigma_{u_L}}{F.S.}\right)\frac{1}{\sqrt{\left\{\xi^2\bar{g}^2 + \bar{f}^2 - \bar{g}\cdot\bar{f}\right\}}} \tag{45}$$

and

$$\omega_{\text{limit}} = \sqrt{\left(\frac{\sigma_{u_L}}{(F.S.)\rho}\right)\frac{1}{b^2\sqrt{\left\{\xi^2 g^2 + f^2 - g\cdot f\right\}}}} \tag{46}$$

respectively. Where $F.S.$ is the factor of safety imposed, g and f were define previously, see equations (36) and (37) for the case of pure rotation, and now

$$\bar{g}(\beta, R_m, \lambda) = \left\{\frac{1}{\left[\left(\frac{b}{a}\right)^{2\sqrt{\frac{1}{\beta}}} - 1\right]}\left(\frac{r}{a}\right)^{\left(-1+\sqrt{\frac{1}{\beta}}\right)} - \frac{\left(\left(\frac{b}{a}\right)^{2\sqrt{\frac{1}{\beta}}}\right)}{\left[\left(\frac{b}{a}\right)^{2\sqrt{\frac{1}{\beta}}} - 1\right]}\left(\frac{r}{a}\right)^{-\left(1+\sqrt{\frac{1}{\beta}}\right)}\right\} \tag{47}$$

and

$$\bar{f}(\beta, R_m, \lambda) = \left\{\sqrt{\frac{1}{\beta}}\frac{1}{\left[\left(\frac{b}{a}\right)^{2\sqrt{\frac{1}{\beta}}} - 1\right]}\left(\frac{r}{b}\right)^{\left(-1+\sqrt{\frac{1}{\beta}}\right)} + \sqrt{\frac{1}{\beta}}\frac{\left(\left(\frac{b}{a}\right)^{2\sqrt{\frac{1}{\beta}}}\right)}{\left[\left(\frac{b}{a}\right)^{2\sqrt{\frac{1}{\beta}}} - 1\right]}\left(\frac{r}{a}\right)^{-\left(1+\sqrt{\frac{1}{\beta}}\right)}\right\} \tag{48}$$

are taken directly from Arnold (ref. 175) for the case of internal pressure. The above first fracture based limits can be considered lower bounds on the corresponding limit loads, particularly for brittle like materials (e.g., PMC). However, in the case of more ductile materials (e.g., TMCs) one would prefer to employ plastic limit analysis to obtain a set of bounds.

5.1.2 Fully-Plastic Limit.—Considering the case of the fully plastic, limit (burst) load (e.g., pressure or speed), extensive studies have been made previously for the case of isotropic tubes and disks under pressure and rotation; see Hill (ref. 183) and Nadai (ref. 184). Following these approaches, applications for the extended case of material transverse anisotropy under pressure for (plane-strain) cylinders and thin disks, were reported in Robinson and Pastor (ref. 185). A generalization of this anisotropic case under rotation will be outlined here. For convenience, we first summarize the governing equations of the present limit load problem, and outline the solution procedure. This will then be followed by a summary of the various proposals for the different limit loads. More detailed studies and derivations can be found in references 184 to 187.

The required three conditions for the limit load solution are the satisfaction of (i) equilibrium (see eq. (1)) and any associated stress boundary conditions, (ii) compatibility for the "plastic" strain rates (see eq. (3)), and iii) the yield function (see eq. (59)). In particular when equilibrium and yield are combined we get for the generalized case of plane strain stress the following general equilibrium expression:

$$\frac{d\sigma_r}{dr} + \frac{1}{r}\left\{1 + \frac{\bar{b}}{2\bar{a}}\right\}\sigma_r - \frac{1}{r}\left[\frac{\sqrt{4\bar{a}K^2 + \{\bar{b}^2 - 4\bar{a}\bar{c}\}\sigma_r^2}}{2\bar{a}r}\right] + \rho\omega^2 r = 0 \tag{49}$$

where

$$\bar{a} = \frac{z_2^2}{2} + \frac{z_4^2}{2} - \frac{(3\zeta - 2)}{4}z_5^2$$

$$\bar{b} = z_1 z_2 + z_3 z_4 - \frac{(3\zeta - 2)}{2}z_5 z_6$$

$$\bar{c} = \frac{z_1^2}{2} + \frac{z_3^2}{2} - \frac{(3\zeta - 2)}{4}z_6^2$$

and

$$z_1 = \frac{(2 - \lambda_1)}{3} \quad z_2 = \frac{-(1 + \lambda_2)}{3}$$

$$z_3 = \frac{(2\lambda_1 - 1)}{3} \quad z_4 = \frac{(2\lambda_2 - 1)}{3} \tag{50}$$

$$z_5 = \frac{(2 - \lambda_2)}{3} \quad z_6 = \frac{-(1 + \lambda_1)}{3}$$

with λ_1 and λ_2 defined for the case of plane stress and plane strain as follows:

Plane Stress: $\lambda_1 = \lambda_2 = 0$

Plane Strain: $\lambda_1 = \frac{2 + \zeta}{4 - \zeta} \quad \lambda_2 = \frac{2(1 - \zeta)}{4 - \zeta}$

Note the strength of anisotropy (ζ) is defined as, $\zeta = 4(\xi^2 - 1)/(4\xi^2 - 1)$, where $\xi = \sigma_{u_L}/\sigma_{u_T}$ is the ratio of longitudinal to transverse yield (or ultimate) stress. Similarly, the required kinematic constraint is the satisfaction of strain compatibility, that is:

$$\dot{\varepsilon}_r = \frac{d}{dr}(r\dot{\varepsilon}_\theta) \tag{51}$$

Finally, the yield (or ultimate) transverse shear stress, K, (first used in eq. (49)) is related to the longitudinal tensile yield stress by the following expression,

$$K^2 = \frac{(\sigma_L^y)^2}{4\xi^2 - 1} = \frac{(\sigma_L^y)^2}{\frac{(4 - \zeta)}{(1 - \zeta)} - 1} \tag{52}$$

Internal Pressure: As an example, for the case of internal pressure only, under plane stress, the final expression (including stress boundary conditions) for the lower bound of failure obtained from equation (49) will be:

$$\int_{\frac{-P_{\text{limit}}}{2K}}^{0} \frac{2d\eta}{\sqrt{\frac{3}{1-\zeta}(1-\eta^2)}-\eta} = \ln\left(\frac{b}{a}\right); \qquad \frac{-P_{\text{limit}}}{2K} \leq 1 \tag{53}$$

where generally this integration requires a numerical procedure. However, for the special case of plane strain under internal pressure only, analytical integration (between $r = a$, $\sigma_r(a) = -P_{\text{limit}}$, and $r = b$, $\sigma_r(b) = 0$) is possible leading to the following lower bound solution.

$$\frac{P_{\text{limit}}}{2K} = \frac{1}{2}\sqrt{\frac{4-\zeta}{1-\zeta}} \ln\frac{b}{a} \tag{54}$$

It is also interesting to note the fact that the above solution also satisfies compatibility thus making it the "exact" limit pressure for the plane strain case and consequently a valid upper bound for the case of plane stress, as discussed by Robinson and Pastor (ref. 185).

Rotation: In the case of rotation (i.e., nonzero body-force term) the resulting differential equations for the lower bound estimates for both the cases of plane-strain and plane-stress are not separable and must be solved for numerically. A straightforward iterative solution technique can be employed in conjunction with Euler integration until the boundary conditions, $\sigma_r(a) = 0$ and $\sigma_r(b) = 0$, are satisfied explicitly. Unfortunately, in the case of rotation the resulting stress state arising from the solution of equation (49) for the case of plane strain cannot be shown to be associated with a kinematically admissible strain field, as in the case of internal pressure loading. Consequently, both the plane stress and plane strain conditions merely yield lower bound (limit) solutions.

An alternative analytical proposal for the upper, lower, as well as out-of-plane bounds have recently been developed and are described more fully in reference 187 with the final expressions taking on the following forms respectively:

Lower Bound:

$$\frac{\hat{P}}{2K} = (2+\bar{\delta})\sqrt{\frac{3}{4-\zeta}}\left\{\frac{1-\left(\frac{a}{b}\right)^{\bar{\delta}}}{1-\left(\frac{a}{b}\right)^{2+\bar{\delta}}}\right\}\left[1-\left(\frac{a}{b}\right)^2\right] \tag{55}$$

Upper Bound:

$$\frac{\hat{P}}{2K} = \frac{\bar{\lambda}}{\gamma}\left(\frac{3\gamma+1}{\gamma+1}\right)\left\{\frac{1-\left(\frac{a}{b}\right)^{1+\frac{1}{\gamma}}}{1-\left(\frac{a}{b}\right)^{3+\frac{1}{\gamma}}}\right\}\left[1-\left(\frac{a}{b}\right)^2\right] \tag{56}$$

Out of Plane Bound:

$$\frac{\hat{P}}{2K} = \frac{b}{h}\left(1-\left(\frac{a}{b}\right)^2\right) \tag{57}$$

where

$$\bar{\delta} = \sqrt{\frac{4-\zeta}{4-4\zeta}}$$

$$\gamma = \frac{1}{\bar{\delta}-1} \tag{58}$$

$$\bar{\lambda} = \sqrt{1+\gamma+(\bar{\delta}\cdot\gamma)^2}$$

Representative limit (upper and lower bound) curves for a given geometry (i.e., $b/a = 1.8$) are shown in figure 24; that is normalized effective pressure, $\hat{P}/2K$, versus strength of anisotropy, ζ. Note in the case of rotation this effective pressure is defined to be the "equivalent" centripetal load, $\hat{P} = \rho\omega^2(b^2 - a^2)/2$, and in the case of internal pressure this is merely the applied internal pressure, $\hat{P} = P_{in}$.

From figure 24 it is apparent that in the case of rotation the difference between upper and lower bounds is greater than in the case of internal pressure, for slightly anisotropic materials; with the averaged effective centripetal limit load (for an isotropic material, $\zeta = 0$) being just slightly lower ($\hat{P}/2K \approx 0.52$) than the corresponding averaged limit pressure load ($\hat{P}/2K \approx 0.58$). Similarly, as the strength of anisotropy is increased ($\zeta > 0.8$) it is interesting to note (and yet coincidental) that plane strain solution for the case of internal pressure follows closely the average limit speed obtained for the rotation case.

Also, from figure 24 we see that the critical value of reinforcement (referred to by Robinson and Pastor (ref. 185) as the condition of over-reinforcement) for the case of internal pressure occurs at a strength of anisotropy equal to, $\zeta = 0.713$ for a $b/a = 1.8$. This point is denoted in figure 24 by the on-set of the plateau. Whereas in the case of rotation, a potential shear induced out-of-plane mode (see eq. (56)) is identified which is purely dependent upon the ratio of outer radius b, to height h, (or length) of the disk (or cylinder). An insightful design oriented presentation of this out-of-plane mode is shown in figure 25, where it is immediately apparent that the critical height (or length) to avoid (or cause) axial splitting before in-plane failure is dependent upon: (i) the strength of anisotropy, (ii) in-plane geometry of the disk (a/b) and (iii) the ratio of in-plane to out of plane shear flow stress (K/K^*).

These curves are simply obtained by equating a given in-plane bound to that of the out-of-plane bound. Though in actuality the modes will most likely interact in a complex way, following the notion of nonlinear interaction curves. Figure 25(a) corresponds to setting the lower in-plane bound equal to the out-of-plane bound while that of figure 25(b) corresponds to equating the average of the upper and lower in-plane bounds to that of the out-of-plane bound. Examining figure 25 it is clear that in the case of isotropy ($\zeta = 0$) the relative size of the disk (a/b) has a significant impact on the allowable height (h). Whereas, in the case of strongly anisotropic yielding (or failure) behavior, the relative size of the disk is not as important as is the ratio of the in-plane to out-of-plane shear flow stress (K/K^*). Furthermore, one can utilize the results displayed in figure 25 to either design a given disk to fail in-plane before axial splitting takes place (i.e., adjusting $h/b(K/K^*)$ to be below the line) or to make sure that what is believed to be the more benign failure mode of axial splitting takes place prior to the more catastrophic in-plane failure (i.e., selecting an $h/b(K/K^*)$ such that it is above the associated line).

Returning to the case of internal pressure, we see that the condition of over-reinforcement corresponds to a point in which the mode of failure switches from that of overall in-plane to that of localized out-of-plane flow within the vicinity of the inner radius ($r = a$). This alternate upper bound limit is important as it suggests either the maximum amount of reinforcement (volume fraction of fibers) one should utilize or alternatively the maximum relative size of the disk for a given amount of reinforcement. If one were to exceed either of these parameters, see figure 26, the resulting design would be inefficient and the resulting limit pressure would be limited by the value of the allowable transverse shear flow stress of the material, as $\hat{P} = 2K$. For example, in the case of PMC's with relatively high volume fractions of fibers ($\zeta \geq 0.95$), the relative disk size, $\lambda/R_m \leq 0.15$, should be small to ensure in-plane failure. From a practical point of view, it is interesting to note that from such a configuration one has the potential to obtain an accurate measure of the transverse shear flow stress (K), since at burst and for this geometry, $P_{in} = 2K$.

Recall, in section 4 we demonstrated that the stored energy per unit mass increases as the relative size (λ/R_m) of the disk is decreased. Consequently, one might conclude that the most efficient flywheel design is that of a relatively "thin" disk. If thicker disks are to be utilized, than one would naturally desire as high a transverse shear stress (K) as possible; thus suggesting the utilization of some type of 3-D weave so as to increase the transverse flow (ultimate) stress and consequently the controlling limit load of the given disk.

Finally, it is important to realize that the first fracture analysis (using the effective J_2 criterion[1]), initially discussed, provides a minimum lower bound as compared to that coming from the ductile plastic limit analysis, see table XIV. This is consistent with the fact that in the first fracture case yielding (or fracture) is satisfied only at a single point, whereas in the plastic limit analysis yielding (or fracture, depending on the values used in the anisotropic strength measurement, ζ) is satisfied at all points throughout the disk. Consequently, one must be cognizant (when estimating the actual limit load) of whether the material tends to exhibit more ductile or brittle behavior dur-

---

[1] Note that in the case of internal pressure a significant difference between the first fracture limit using maximum hoop stress only verses the effective J_2 criterion is observed (again since radial stress is always compressive the effective J_2 (multiaxial stress measure) is always larger than the hoop stress, maximum stress, alone).

ing failure, which is determined primarily by material selection (e.g. resign/sizing/flow) and the chosen manufacturing process (e.g., cure temperature, environment, etc.). In materials that exhibit both characteristics, interaction effects between brittle and ductile failures become important, therefore this will be an area of future study.

5.2 Fatigue Life

Employing flywheels as energy storage systems inherently demand that the flywheel be repeatedly spun up and down, thus requiring the designer to be concerned about the fatigue capacity of any given flywheel system. To address this concern we will utilize a previously developed transversely isotropic fatigue damage model (refs. 188, 189). This model has a single scalar damage state variable (damage is the same in all directions) that represents both mesoscale-initiation and -propagation of damage but whose rate of accumulation of damage is anisotropic (dependent upon the orientation of the preferred material direction relative to the loading direction). Furthermore, it has both a static fracture limit and endurance limit, accounts for mean stress effects and captures the typically observed nonlinear-cumulative effects in multiple block-program loading tests. The anisotropic fatigue (endurance) limit and static fracture surfaces are comprised of physically meaningful invariants that represent stress states that are likely to strongly influence the various damage modes within composites. For example, (i) the transverse shear stress (I_1)–matrix cracking, (ii) the longitudinal shear stress (I_2)–dictates interfacial degradation, and (iii) the maximum normal stress (I_3) in the fiber direction which dictates fiber breakage. All three of these invariants are combined into a function representing the effective transversely isotropic J_2 invariant:

$$F_{()} = \sqrt{\frac{1}{()_L}\left\{(4\xi_{()}^2 - 1)I_1 + \frac{(4\xi_{()}^2 - 1)}{\eta_{()}^2}I_2 + \frac{9}{4}I_3\right\}} \tag{59}$$

where

$$I_1 = J_2 - \hat{I} + \frac{1}{4}I_3$$
$$I_2 = \hat{I} - I_3$$
$$I_3 = I^2$$

in which

$$J_2 = \frac{1}{2}S_{ij}S_{ij}$$
$$I = D_{ij}S_{ij}$$
$$\hat{I} = D_{ij}S_{jk}S_{ki}$$
$$D_{ij} = d_i d_j$$
$$S_{ij} = \sigma_{ij} - \frac{1}{3}\sigma_{kk}\delta_{ij}$$

and d_i ($i = 1,2,3$) are the components of a unit vector denoting the local fiber direction. Note this effective J_2 invariant (eq. (59)) has been the multiaxial criterion used throughout this study, but specialized to the pertinent case of circumferential reinforcement with $\eta = 1$ (equal longitudinal and transverse shear response). This special case is simply written in terms of the radial and hoop stress as follows:

$$F_{()} = \sqrt{\frac{1}{()_L}\left\{\xi^2_{()}\sigma_r^2 + \sigma_\theta^2 - \sigma_r\sigma_\theta\right\}} \tag{60}$$

where the open bracket subscript notation in equation (59) and the above is used to distinguish between the static fracture, endurance limit and normalization surfaces, see reference 189.

This fatigue model has already been successfully applied to the problem of a circumferentially reinforced disk subjected to internal pressure, see (refs. 190 and 191). Consequently, here we will focus our attention only on the fatigue life of a circumferentially reinforced, rotating disk and in particular on the influence of the key geometric parameters, i.e., mean radius and thickness. The fatigue life model of (ref. 188) requires at a minimum the availability of both longitudinal and transverse S-N curves to describe the evolution of damage for a given material system. As this data is presently not available for the PMC system of interest we will confine our investigation to a previously examined SiC/Ti system; the associated damage model parameters being completely defined in reference (ref. 191).

Results for the case of a single, matrix cladded (inner and outer monolithic disk), disk subjected to multiple cycles of rotational loading (triangular waveform) is shown in figures 27 to 29. In figure 27 the limit burst speed versus the geometry of the disk is presented, wherein this limit speed corresponds to a given induced stress state at the various radial locations (i.e., inner radius (ID) and outer radius (OD)) that fulfills the static fracture condition of equation (51), that is $F_L - 1 = 0$. This analysis is defined as an uncoupled approach, see reference 190. Figure 27(a) clearly shows that the limit speed greatly decreases with increasing mean radius; while figure 27(b) illustrates that as the relative thickness (λ/R_m) of the disk compared to the mean radius increases the difference between the inner and outer limit speed increases greatly as well, as one would expect. In figure 28, the resulting speed versus cycles to failure curve defining fatigue initiation at the inner radius (ID) of the composite core for various mean radii are displayed. Again, we observe the expected trend associated with increasing the mean radius of the disk; that is, a marked decrease in either the limit speed (for similar life times) or number of cycles to end of life (for the same speed). If one where to normalize the calculated fatigue limit speed with the corresponding static limit (burst) speed at the same radial location for the given geometry one can obtain a master fatigue initiation life curve that is essentially independent of mean radius variation, see figure 29. A similar master curve can be obtained corresponding to fatigue initiation at other radial locations within the disk as well. Also, if one were to conduct a coupled deformation and fatigue damage analysis, as done previously for the case of internal pressure (see refs. 190 and 191) a single master design life curve representing the global failure of the disk due to fatigue could be produced. Such a curve will be produced in the near future for the PMC reinforced disks of interest to the RSL program when the necessary experimental data for characterizing the current life model become available.

6.0 CONCLUSIONS

In this study we have attempted to put into perspective the problem of a rotating disk, be it a single disk or a number of concentric disks forming a unit. An analytical model capable of performing an elastic stress analysis for single/multiple, annular/solid, anisotropic/isotropic disk systems, subjected to both pressure surface tractions, body forces (in the form of temperature-changes and rotation fields) and interfacial misfits has been derived and discussed. Results of an extensive parametric study were presented to clearly define the key design variables and their associated influence. In general the important parameters are misfit, mean radius, thickness, material property and/or load gradation, and speed; all of which must be simultaneously optimized to achieve the "best" design. All of the observations made herein regarding the deformation analysis are in total agreement with previous conclusions and observations made in the past by other investigators.

Also, the important issue of defining proper performance/merit indices (based on the specific stored energy), in the presence of multiaxiality and material anisotropy have been addressed and utilized to discuss the difference between flywheels made from PMC and TMC materials with either an annular or solid geometry. An interesting observation made is that an annular anisotropic disk is more efficient than its solid counterpart; this is in sharp contrast to the fact that an isotropic solid disk is more efficient than an annular disk.

Finally two major aspects of failure analysis, that is the static and cyclic limit (burst) speeds were addressed. In the case of static limit loads, upper, lower, and out-of-plane bounds for disks with constant thickness were presented for both the case of internal pressure loading (as one would see in a hydroburst test) and pure rotation (as in the case of a free spinning disk). The results (interaction diagrams) were displayed in a designer friendly format. For the case of fatigue, a representative fatigue/life master curve was illustrated in which the normalized limit speed versus number of applied cycles was described for a cladded TMC disk application.

REFERENCES

1. Genta, G.: Kinetic Energy Storage: Theory and Practice of Advanced Flywheel Systems, Butterworths, 1985.
2. Keckler, C.R.; Bechtel, R.T. and Groom, N.J.: "An Assessment of Integrated Flywheel System Technology," NASA CP–2346, 1984.
3. Bitterly, J.G.: "Flywheel Technology," IEEE AES Systems Magazine, 1998.
4. DeTeresa, S.J.: "Materials for Advanced Flywheel Energy Storage Devices," MRS Bulletin, 1999.
5. Kaftanoglu, B.; Soylr, R.; and Oral, S.: "Mechanical Energy Storage Using Flywheels and Design Optimization," from: Energy Storage Systems by B. Kilkis and S. Kakac, Kluwer Academic Publishers, 1989.
6. Grubler, M.: "Ring Spannung and Zugfestigkeit," Z.D.V. Deutsch, Ing., vol. 50, 1906.
7. Donatch, M.: "Die Berechnung Rotierenden Scheiben Und Ringe Nach Einem Neven Verfahren," Springer, 1912.
8. Stodola, A.: Steam and Gas Turbines, McGraw-Hill Book Company, Inc, 1927.
9. Manson, S.S.: The Determination of Elastic Stresses in Gas-Turbine Disks, NACA TN–1279, 1947.
10. Millenson, M.B. and Manson, S.S.: Determination of Stresses in Gas-Turbine Disks Subjected to Plastic Flow and Creep, NACA 906, 1948.
11. Chen P.C.; Brown, J.F.; and McKnight R.L.: Cyclic Elastic/Plastic/Creep Analysis of Rotating Disks–User Manual, GE R78AEG295, 1978.
12. Seireg, A. and Surana, K.S.: "Optimum Design Rotating Disk," J. Engr. for Industry, Trans. of the ASME, vol. 92, 1970, pp. 1–10.
13. Habercom, G.: "Design and Applications of Flywheels." Vol. 1. 1964-Aug., 1978 (Citations from the NTIS Data Base)." NTIS, 1979.
14. Habercom, G.: "Design and Applications of Flywheels." Vol. 2. 1978-Sep., 1979 (Citations from the NTIS Data Base)." NTIS, 1979.
15. Habercom, G.: "Design and Applications of Flywheels." (Citations from the NTIS Data Base). NTIS, 1979.
16. Grammel, R.: "Neue Loesungen des Problems der Rotierenden Schebe," Ing. Arch., vol. 7, 1936.
17. Bisshopp, K.E.: "Stress Coefficients for Rotating Disks of Conical Profile," J. App. Mech., Trans. of the ASME, vol. 11-A, 1944.
18. Leopold, W.R.: "Centrifugal and Thermal Stresses in Rotating Disks," J. Appl. Mech., vol. 16, no. 2, 1949, pp. 213–215.
19. Beck, F.: "Centrifugal Stresses in Disks," Mach Design, vol. 24, no. 51949, pp. 137–143.
20. Prochnitcki, W.: "Approximate Stress Calculation in Rotating Disks," Pszeglad Mech, vol. 22, no. 20, 1963, pp. 213–215.
21. Kumar, B.: "Stress Distribution in Thin Rotating Circular Disk Having Transient Shear Stress Applied on the Outer Edge," J Franklin Inst, vol. 281, no. 4, 1966, pp. 315–323.
22. Mahmoodi, P.: "On Optimum Design of Rotating Disk of Nonuniform Thickness," ASME, 1969.
23. Manna, F.: "Rotating Disks of Unconventional Profile," Meccanica, vol. 3, no. 4, 1968, pp. 274–282.
24. Ranta, M.A.: "On the Optimum Shape of Rotating Disk of Any Isotropic Material," Int. J. Solid. Struct., vol. 5, no. 11, 1969, pp. 1247–1257.
25. Tang, S.: "Note on Acceleration Stress in Rotating Disks," Int. J. Mech. Sci., vol. 12, no. 2, 1970, pp. 205–207.
26. Basak, D.K. and Metwalli, S.M.: "Stress Analysis Compounded Rotating Disks," J. Franklin Inst., vol. 292, 1971, pp. 265–275.
27. Wu, C.: "Asymptotic Solution of a Rotating Disk," ASME Pap 71-APM-Q, 1971
28. Lawson, L.: "Design and Testing of High Energy Density Flywheels for Application to Flywheel/Heat Engine Hybrid Vehicle Drives," Intersociety energy convention eng conf, 1971, Paper 719150, pp. 1142–1150.
29. Holland, M.: "Radial-Displacement Solution for a Rotating Disk With a Hyperbolic Thickness Profile," J. Strain Anal., vol. 7, no. 1, 1972, pp. 7–8.
30. Laczkowski, R.: "Distribution in a Rotating Disk of Variable Thickness," Przegl Mech., vol. 32, no. 3, 1973, pp. 93–96.
31. Potemkina, A.M.; Kodner, M. Ya; Kushnerov, E.A. and Andreeva, N.P.: "Problem of Strength of Non-Uniformly Heated Rotating Disk," Probl Prochn, vol. 5, no. 5, 1973, pp. 18–23.
32. Feng, W.: "On Rubber Disks Under Rotation or Axisymmetric Stretching," Int J Non-Linear Mech, vol. 8, no. 6, 1973, pp. 539–550.

33. Georgian, J.: "Dimensionless Sum and Difference Stress Charts for Rotating and Stationary Disks," ASME, Des. Eng. Div., 1974.

34. Kirkhope, J. and Wilson, G.: "Vibration and Stress Analysis of Thin Rotating Disks Using Annular Finite Element," J. Sound Vib., vol. 44, no. 4, 1976, pp. 461–474.

35. Chattopadyay, T.K. and Bhattacharyya, A.: "Analysis of Rotating Disk Using the Finite Element Method," J. Inst. (India) Mech. Eng. Div., vol. 57, pt. ME, 1, 1976, pp. 13–17.

36. Haddow, J.B. and Faulkner, M.G.: "Finite Elastic Deformation of an Annular Rotating Disk," J. Eng. Mater. Technol. Trans. ASME, vol. 98, no. 4, 1976, pp. 375–379.

37. Curtis, D.M. and Berger, B.S.: "Optimum Design of the Homogeneous Plane-Stress Flywheel," ASME Pap, no. 77, DET 112, for Meet, 1977.

38. Miller, A.K.: "Structural Modeling of a Thick-Rim Rotor," DOE CONF–781046, 1978, pp. 93–98.

39. Prasek, L.: "Calculation of Distribution of State of Stress in Rotating Disks," Rev. Roum. Sci. Tech. Ser. Mec. Appl., vol. 23, no. 5, 1978, pp. 755–778.

40. Bullion, T.M.; Zowarka, R.; Driga, M.D.; Gully, J.H.; Rylander, H.G.; Tolk, K.M.; Weldon, W.F.; and Woodson, H.H.: "Testing and Analysis of Fast Discharge Homopolar Machine (FDX)," IEEE Cat no. 79CH1505-7, 1979, pp. 333–342.

41. Abir, A. and Fisher, U.: "Three-Dimensional Stress and Deformation Analysis of Rotating Finned Bodies," Isr. J. Technol., vol. 17, no. 2, 1979, pp. 67–77.

42. Irie, T.; Yamada, G.; and Aomura, S.: "Steady-State Response of a Rotating Damped Disk of Variable Thickness," J. Appl. Mech. Trans. ASME, vol. 47, no. 4, 1980, pp. 896–900.

43. Nigh, G.L. and Olson, M.D.: "Finite Element Analysis of a Rotating Disk," J. Sound Vib., vol. 77, no. 1, 1981, pp. 61–78.

44. Sandgren, E. and Ragsdell, K.M.: "Optimal Flywheel Design with a General Thickness Form Representation," J. Mech. Transm. Autom. Des., vol. 105, no. 3, 1983, pp. 425–433.

45. Karpov, A.V.: "Analysis of Isotropic Three-Layer Disk Stress State," Sov. Aeronaut., vol. 26, no. 2, 1983, pp. 106–111.

46. Shanbhag, M.R.: "Stress Analysis of Rotating Disk with FEA–Emphasis on Stresses at Contours of Dissimilar Holes at the Rim," Comput. Struct., vol. 18, no. 4, 1984, pp. 603–608.

47. Selvadurai, A.P.S. and Singh, B.M.: "Some Annular Disk Inclusion Problems in Elasticity," Int. J. Solids and Struct., vol. 20, no. 2, 1984, pp. 129–139.

48. Nowinski, J.L.: "Note on the Solution of the Equations Controlling Stability of Nonlinear Thermoelasic Waves in a Spinning Disk," J. Therm. Stresses, vol. 7, no. 1, 1984, pp. 75–78.

49. Lobodov, V.V. and Bolotov, A.M.: "Behavior of a Rotating Elliptical Ring of Variable Section," Porbl Prochn, no. 2, 1987, pp. 22–25.

50. Berger, M. and Porat, J.: "Optimal Design of a Rotating Disk for Kinetic Energy Storage," J. Appl. Mech. Trans. ASME, vol. 55, no. 1, 1988, pp. 164–170.

51. Von Burg, P.; Widmer, J.; Asper, H.K.; Grieder, T.; and Riessen, H.J.: "Comparison of the Predicted and Measured Dynamic Behavior of High Speed Spinning Rotors," IEEE, 1988, pp. 93–95.

52. Flanagan, R.C.; Aleong, C.; Anderson, W.M.; and Olberman, J.: "Design of a Flywheel Surge Power Unit for Electric Vehicle Drives," IEEE Cat no 90CH2942-1,1990, pp. 211–217.

53. Bolotov, A.M.; Voronov, V.P.; and Lobodov, V.V.: "Strength Calculation of a Shell Flywheel Under the action of Operational Loads," Probl. Prochn., no. 7, 1991, pp. 80–84.

54. Renshaw, A.A. and Mote, C.D.: "Absence of One Nodal Diameter Critical Speed Modes in an Axisymmetric Rotating Disk," J. Appl. Mech. Trans. ASME, vol. 59, no. 3, 1992, pp. 687–688.

55. Kai-Yuan, Y. and Han, R.P.S.: "Analysis of High-Speed Rotating Disks with Variable Thickness and Inhomogeneity," J. Appl. Mech., vol. 61, 1994, pp. 186–191.

56. Carrier G.F.: "Provided Stress Analysis for the Case of Anisotropic Rotating Disks of Uniform Thickness," Trans ASME, vol. 65, 1943.

57. Sen Gupta A.M., and Bull, Calcutta: "Provided the Stress Analysis for Certain Types of Anisotropic Rotating Disks of Uniform Thickness," Math. Soc., vol. 41, 1949.

58. Lekhnitskii, S.: Theory of Elasticity of an Anisotropic Elastic Body, Holden Day, New York, 1963.

59. Samanta, B.K.:" Stresses in Anisotropic Non-Homogeneous Rotating Circular Disk of Variable Thickness," Rev Roumaine Des Sciences Techniques-Serie De Mecccanique Appliquee, vol. 11, no. 2, 1966, pp. 503–511.

60. Morganthaler, G.F.; and Bonk, S.P.: "Composite Flywheel Stress Analysis and Material Study," SAMPLE Nat. Symposium 12th, 1967.

61. Chakrabarti, S.K.: "Plane Thermal Stress in Non-Homogeneous Transversely Isotropic Rotating Circular Disk," Serie de Mecanique Appliquee, vol. 13, no. 5, 1968, pp. 923–928.

62. Tang, S.: "Elastic Stress in Rotating Anisotropic Disks," Int. J. Mech. Science, vol. 11, no. 6, 1969, pp. 509–517.

63. Murthy, N.S. and Sherbourne, A.N.: "Elastic Stresses in Anisotropic Disks of Variable Thickness," Int. J. Mech. Sci., vol. 12, no. 7, 1970, pp. 627–640.

64. Lakshminarayana, H.V. and Srinath, H.: "Elastic Stresses in Rotating Orthotropic Disks of Variable Thickness," J. Strain Anal., vol. 8, no. 3, 1973, pp. 176–181.

65. Sandman, B.E.: "Finite Deformation of Rotating Orthotropic Cylinder with Linear Elasticity," Comput. Struct., vol. 4, no. 3, 1974, pp. 581–591.

66. Toland, R.H. and Alper, J.: "Transfer Matrix for Analysis of Composite Flywheels," J. Compos. Mater., vol. 10, 1976, pp. 258–261.

67. Gurushankar, G.V.: "Thermal Stresses in a Rotating, Nonhomogeneous, Anisotropic Disk of Varying Thickness and Density," J. Strain Anal., vol. 10, no. 3, 1975, pp. 167–171.

68. Chang, C.I.: "Stresses and Displacements in Rotating Anisotropic Disks with Variable Densities," AIAA J., vol. 14, no. 1, 1976, pp. 116–118.

69. Crivelli, V.I.; Rodriquez, F.; Sorrentino, V.; and Volpe, G.P.: "Use of Composite Materials in Designing High Energy Flywheels-1,"Quad Ric Progettazione, no. 5, 1976, pp. 159–163.

70. Huntington, R.A. and Kirk, J.A.: "Stress Redistribution for the Multiring Flywheel," ASME Paper, No. 77-WA/DE-26, 1977.

71. Christensen, R.M. and Wu, E.M.: "Optimal Design of Anisotropic (Fiber–Reinforced) Flywheels," J. Compos. Mater., vol. 11, 1977, pp. 395–404.

72. Danfelt, E.L.; Hews, S.A.; and Chov, T.: "Optimization of Composite Flywheel Design," Int. J. Mech. Sci., vol. 19, 1977, pp. 69–78.

73. Rolston, J.A.: "Fiber Glass Super Flywheels," SAMPE Q, vol. 8, no. 2, 1977, pp. 7–12.

74. Dick, W.E.: "Design and Manufacturing Considerations for Composite Flywheels," Supt. of Doc., GPO, pp. 276–287.

75. Shiratory, E.; Ikegami, K.; and Hattori, T.: "Rotating Strength of Circumferentially Fiber-Reinforced Composite Disks," Bull JSME, vol. 21, no. 153, 1978, pp. 381–388.

76. Reedy, E.D., Jr.: "Sandia Composite-Rim Flywheel Development," NTIS, 1978, pp. 87–91.

77. Davis, D.E.: "Advanced Composite Flywheel for Vehicle Application," NTIS, 1978, pp. 164–170.

78. Satchwell, D.L.: "High-Energy-Density Flywheel," NTIS, 1978, pp. 172–175.

79. Lustenader, E.L.; Hickey, J.S.; Nial, W.R.; Plunkett, A.B.; Richter, E.; Turnbull, F.G.; and Chang, G.: "Laboratory Evaluation of a Composite Flywheel Energy Storage," IEEE Cat No. 78-CH1372-2 ENERGY, vol. 2, 1978, pp. 984–991.

80. Rabenhorst, D.W.: "Low Cost Flywheel Demonstration," NTIS, 1978, pp. 44–54.

81. Reedy, E.D. Jr. and Street, H.K.: "Composite-Rim Flywheel Spin Test," SAMPE Q, vol. 10, no. 3, 1979, pp. 36–41.

82. Baer, M.R.: "Aerodynamic Heating of High-Speed Flywheels in Low-Density Environments," NTIS, 1978, pp. 99–107.

83. Hattori, T.; Ikegami, K.; and Shiratori, E.: "Rotating Strength of Glass-Carbon Fiber-Reinforced Hybrid Composite Disks," Bull JSME, vol. 21, no. 161, 1978, pp. 1595–1601.

84. Belingardi, G.; Genta, G.; and Gola, M.: "Study of the Stress Distribution in Rotating, Orthotropic Disks," Composites, vol. 10, no. 2, 1979, pp. 77–80.

85. Nimmer, R.P.: "Laminated Flywheel Disk with Filament Wound Outer Ring," NTIS, 1979, pp. 399–406.

86. Biermann, J.W.: "Hybrid Drives with Flywheel-Type Energy Storage," OZE Oesterr Z Elektr, vol. 32, no. 7, 1979, pp. 331–336.

87. Miller, A.K.: "Recent Spin Test of Two Composite Wagon Wheel Flywheels," NTIS, 1979, pp. 347–355.

88. Mishra, C.B. and Shrivastava, A.K.: "Stresses in Rotating Composite Inhomogeneous Disk of Variable Thickness with Axial Hole," Rev. Roum. Sci. Tech. Ser. Mec. Appl., vol. 24, no. 3, 1979, pp. 415–425.

89. Kulkarni, S.V.: "Flywheel Rotor and Containment Technology Development Program of the United States Department of Energy," Int. Conf. on Compos. Mater., 1980.

90. Nimmer, R.: "Alpha-Ply Laminated-Disc Flywheel Rotor," Department of Defense (United States), 1980.
91. Tsuda, Sh.; Shiratory, E.; and Ikegami, K.: "Rotating Strength of Laminated Composite Disk," Bull JSME, vol. 23, no. 180, 1980, pp. 822–830.
92. Ari-Gur, J. and Stavsky, Y.: "On Rotating Polar-Orthotropic Circular Disks," Int. J. Solids Struct., vol. 17, no. 1, 1981, pp. 57–67.
93. Genta, G. and Gola, M.: "Stress Distribution of Orthotropic Rotating Disk," J. Appl. Mech. Trans. ASME, vol. 48, no. 3, 1981, pp. 559–562.
94. Daniel, W.J.T.: "Flywheel Design by the Finite Element Method," Mech. Eng. Trans. Inst Eng. Aust., vol. ME7, no. 2, 1982, pp. 75–79.
95. Genta, G.: "Spin Test of Medium Energy Flywheel," Composites, vol. 13, no. 1, 1982, pp. 36–46.
96. Coppa, A.: "Composite Hybrid Flywheel Design Optimization and Fabrication," In Courtesy Assoc., Inc. Proc. of the DOE Phys. and Chem. Storage Ann. Contractors' Rev. Meeting (SEE N83–28586 17–44), 1982, pp. 255–262.
97. Kozlov, I.A.; Leshchenko, V.M.; and Yudin, A.B.: "Experimental Investigation of Stress-Strained State and Load-Carrying Capacity of Flywheel Model of Energy Accumulators from Composite Material," Probl. Prochn., no. 8 (158), 1982, pp. 22–25.
98. Ikegami, K.; Igarasi, J.; and Shiratori, E.: "Composite Flywheel with Rim and Hub," Int. J. Mech. Sci., vol. 25, no. 1, 1983, pp. 59–69.
99. Ferrero, C.; Genta, G.; and Marinari, C.: "Experimental Strain Measurements on Bare Filament Flywheel," Composites, vol. 14, no. 4, 1983, pp. 359–364.
100. Misra, J.C. and Achari, R.M.: "Thermal Stresses in Orthotropic Disk due to Rotating Heat Source," J. Therm Stresses, vol. 6, no. 2–4, 1983, pp. 115–123.
101. Leshchenko, V.M.; Kosov, I.; and Kozlov, I.A.: "Stress-Strain and Limit State of Composite Flywheels with Spokes, Communications 1. Analytical Relations," Probl. Prochn., no. 8, 1985, pp. 98–102.
102. Ferrero, C.; Genta, G.; Marinari, C.; and Ronco, C. "Experimental Study of the Stress Distribution in the Spokes of Bare Filament Flywheel," Composites, vol. 16, no. 4, 1985, pp. 286–292.
103. Moorlat, P.A. and Portnov, G.G.: "Analysis of the Energy Capacity of Rim-Spoke Composite Flywheel," Mech. Compos. Mater., vol. 21, no. 5, 1985, pp. 594–599.
104. Valiulin, A.Kh; Mukhambetzhanov, S.G.; Antsilevich, Ya.G.; and Golovanov, A.I.: "Analysis of Fiber-Reinforced Composite Flywheel by the Finite Element Method," Probl. Prochn., no. 6, 1987, pp. 12–17.
105. Widmer, J.; Genta, G.; von Burg, P.; Asper, H.; and Hans, K.: "Prediction of the Dynamic Behavior of a Flywheel Rotor System by FE-Method," IEEE, 1988, pp. 97–104.
106. Antsilevich, Ya. G.; Valiullin, A.Kh.; and Cherevatskii, S.B.: "Application of Finite-Element Method in the Calculation of Combined Composite Flywheel," Mech. Compos. Mater., vol. 23, no. 6, 1988, pp. 737–743.
107. Portnov, G.G. and Kustova, I.A.: "Energy Capacity of Composite Flywheel with Continuous Chord Winding," Mech. Comp. Mat., vol. 24, no. 5, 1989, pp. 688–694.
108. Portnov, G.G.; Kustova, I.A.: "Metal-Composite Flywheel with the Specified Limiting Angular Rotational Speed," Mech. Comp. Mater., vol. 24, no. 3, 1988, pp. 400–406.
109. Moorlat, P.A.; Portnov, G.G.; and Ryazanov, A.P.: "Analysis of the Energy Capacity of Rim-Spoke Flywheels," Mech. Compos. Mater., vol. 27, no. 3, 1991, pp. 318–326.
110. Portnov, G.G.; Kulcov, V.L.; Lappo, V.A.: "Energy Storage Capacity of Flywheel with Laminated Quassi-Isotropic or Isotropic Central Disk," Mekh Kompoz Mater., vol. 29, no. 1, 1993, pp. 35–49.
111. Portnov, G.G.; Mungalov, D.D.; and Barinov, I.N.: "Evaluation of Resistance of Composite Rim Flywheels to Radial Tensile Inertial Stresses Basing on Data of Loading a Rim Segment in Pure Bending," Mekh Kompoz Mater., vol. 29, no. 4, 1993, pp. 521–526.
112. Watanabe, M. and Ogita, H.: "Evaluation of Ceramic Rotor Strength by Cold And Hot Spin Tests," ASME 94-GT-460, 1994, pp. 1–8.
113. Tutuncu, N.: "Effect of Anisotropy on Stresses in Rotating Disks," Int. J. Mech. Sci., vol. 37, 1995, pp. 873–881.
114. Christopher, D.A.; Beach, R.F.; and Barton, J.R.: "Flywheel Energy Storage System Test on the International Space Station," IEEE, 1997, pp. 1762–1766.
115. Weissbach, R.S.; Karady, G.G.; and Farmer, R.G.: "Model and Simulation of a Flywheel Energy Storage System at a Utility Substation Using an Induction Machine," Illinois Inst. of Technology, 1998, pp. 906–910.

116. Sung, K.Ha; Hee-Moon J.; and Young-Soo Ch.: "Optimum Design of Thick-Walled Composite Rings for an Energy Storage System," J. Comp. Mat., vol. 32, no. 9, 1998, pp. 851–73.

117. Silva, A.D. and Grilo, E.C.: "Plastic Deformation of Rotating Disk of Uniform Thickness," Tecnica (Lisbon), vol. 45, no. 398, 1970, pp. 413–416.

118. Amanda, S.: "Elasto-Plastic Stress Analysis of Disks Subjected to Transient Thermal and Centrifugal Loadings," Proc. 14th Jap Congron Mater. Res., 1970, pp. 83–86.

119. Shevchenko, Yu.N.; Terekhov, R.G.; and Borisyuk, A.I.: "Experimental Check of the Applicability of the Theory of Small Elastoplastic Deformations to the Design of Revoluting Disks," Prikl Mekh, vol. 9, no. 1, 1973, pp. 57–60.

120. Weber, H. and Wawra, H.: "Calculation of Partly Plasticized Rotating Circular Disks of Reinforced Material by Means of an Analog Computer," Forsck Ingenieurwes, vol. 38, no. 4, 1972, pp. 118–117.

121. Pisarenko, G.S. and Rogozina, L.V.: "Problem of Investigation of the Supporting Power of Rotating Disks by the Method of Optically-Sensitive Coatings," Probl. Prochn., vol. 5, no. 1, 1973, pp. 73–77.

122. Reid, S.R.: "On the Influence of the Acceleration Stresses on the Yielding of Disks of Uniform Thickness," Int. J. Mech. Sci., vol. 14, no. 11, 1972, pp. 755–763.

123. Ginesu, F.; Picasso, B.; and Priolo, P.: "Elasto-Plastic Analysis of a Rotating Model Conical Turbine Disk," J. Strain Anal., vol. 10, no. 3, 1975, pp. 167–171.

124. Amanda, S.: "Non-Linear Boundary Value Problem of Elasto-Plasticity in Centrifugal Force Field," JSME, 1975, pp. 261–266.

125. Kozlov, I.A. and Bogaichuk, V.I.: "Investigation of the Strength of Rotating Disk at Low Temperatures," Probl. Prochn., no. 4, 1976, pp. 43–47.

126. Lishka, T. and Zyczkowski, M.: "Optimum Design of Nonuniformly Heated Rotating Disks with Allowance for Their Elastic and Limit Load-Bearing Capacity," Mech. Teo i Stosow, vol. 14, no. 2, 1976, pp. 283–302.

127. Gururaja, K. and Srinath, H.: "Elasto-Plastic Analysis of an Anisotropic Rotating Disk of Variable Thickness," J. Inst. Eng. (India) Mech. Eng. Div., vol. 57, pt. ME 5, 1977, pp. 243–246.

128. Anad, S.C. and Shaw, H.: "Elastic-Plastic Analysis of a Rolling Disk by Finite Elements," Int. J. Mech. Sci., vol. 19, no. 1, 1977, pp. 37–44.

129. Tvergaard, V.: "On the Burst Strength and Necking Behavior of Rotating Disks," Int. J. Mech. Sci., vol. 20, no. 2, 1978, pp. 109–120.

130. Feng, W.W.: "Finite Deformation of Anisotropic Plastic Rotating Disks," AIAA J., vol. 16, no. 11, 1978, pp. 1205–1207.

131. Gamer, U.: "Tresca's Yield Condition and the Rotating Disk," J. Appl. Mech. Trans. ASME, vol. 50, no. 3, 1983, pp. 676–678.

132. Gamer, U.: "Rotating Solid Disk in the Fully Plastic State," Forsch Ingenieurwes, vol. 50, no. 5, 1984, pp. 137–140.

133. Zowczak, W.: "On Plastic Design of Rotating Disks of Finite Thickness," Rozpr Inz, vol. 32, no. 3, 1984, pp. 439–447.

134. Mack, W. and Gamer, U.: "Stress Distribution in a Elasto-Plastic Circular Caused by a Circular Heat Source," Forsch Ingenieurwes, vol. 51, no. 5, 1985, pp. 160–164.

135. Liu, X.: "Measurement of Elastoplastic Stresses of Rotating Disk in Hot State," J Aerospace Power Hangkong Dongli Xuebao, vol. 5, no. 4, 1990, pp. 292–296.

136. Gueven, U.: "Elastic-Plastic Stresses in a Rotating Annular Disk of Variable Thickness and Variable Density," Int. J. Mech. Sci., vol. 34, no. 2, 1992, pp. 133–138.

137. Megahed, M.M. and AbdelKader, M.S.: "Elastoplastic Analysis of Rotating Shrink-Fitted Disks with Nonlinear Hardening Characteristics," In J. Solid Struct., vol. 30, no. 6, 1993, pp. 751–765.

138. Wu, G. and Zhang, X.: "Variational Method of Solution About Rotating Disk in Elastic-Plastic Range with Arbitrary Hardening Behavior," Beijing Hangkong Hangtian Daxue Xuebao, no. 2, 1993, pp. 61–67.

139. You, L.H.; Long, S.Y.; and Zhang, J.J.: "Perturbation Solution of Rotating Solid Disks with Nonlinear Strain-Hardening," Mech. Res. Commun., vol. 24, no. 6, 1997, pp. 649–658.

140. Parmaksizoglu, C. and Guven, U.: "Plastic Stress Distribution in a Rotating Disk with Rigid Inclusion Under a Radial Temperature Gradient," Mech. Struct. Mach., vol. 26, no. 1, 1998, pp. 9–20.

141. Shrzypek, J.J.: Plasticity and Creep: Theory, Examples and Problems, R.B. Hetnarski, English Editor, CRC Press, 1993.

142. Shoemaker, E.M.: "Creep Rupture of Rotating Disks and Thin Shells of Revolution," J. Appl. Mech., vol. 32, no. 3, 1965, pp. 507–510.

143. Ma, B.M.: "Power-Function Creep Analysis for Rotating Solid Disks Having Variable Thickness and Temperature," Franklin Inst. J., vol. 277, no. 6, 1964, pp. 593–612.

144. Kossecki, J.: "Generalized Plane State of Stress in Rotating Viscoelastic Disk with Elastic Loop," Polska Akademia Nauk-rozpravy Inzynierskie, vol. 12, no. 2, 1964, pp. 297–307.

145. Townley, C.H.A.: "Use of Computer in the creep Analysis of Power Plant Structures," Appl. Sci. Publ. Ltd., 1971.

146. Hayhurst, D.R.: "Prediction of Creep-Rupture Times of Rotating Disks Using Biaxial Damage Relationships," J. Appl. Mech., Trans. ASME, vol. 40, no. 4, 1973, pp. 915–920.

147. Lenard, J.G.: "Analysis of the Secondary Creep of a Rotating Flat Disk," Trans. Can Soc. Mech. Eng., vol. 1, no. 4, 1972, pp. 227–228.

148. Sosnin, O.V. and Gorev, B.V.: "Energy Variant of the Theory of Creep and Long-Time Strength-3. Creep and Long-Time Strength of Rotating Disks," Probl. Prochn., vol. 6, no. 3, 1974, pp. 3–7.

149. Dem'yanushko, I.V. and Temis, Yu.M.: "Kinetics of the State of Stress and Strain of Disks Under Cyclic Non-Isothermal Loading," Izv Nauk (SSSR) Mekh Trerd Tela, no. 3, 1975, pp. 90–98.

150. Gupta, S.K: "Analysis of Rotating Disk of Orthotropic Material in the Theory of Creep," J. Inst. Eng. (India) Mech. Eng. Div., vol. 58, pt. ME 1, 1977, pp. 1–4.

151. Nikitenko, A.F.: "Determination of Critical Number of Rotations for an Equistrong Disk in the Process of Creep," Probl. Prochn., no. 8 (158), 1982, pp. 15–18.

152. Mukhopadhyaya, A.K.: "Time-Hardening and Time-Softening Non-Homogeneous Rotating Circular Elastic Plate," Rev. Roum. Sci. Tech. Ser. Mec. Appl., vol. 28, no. 6, 1983, pp. 633–641.

153. Misra, J.C. and Samanta, S.C.: "Thermal Stresses in Rotating Disks of Thermorheologically Simple Solids," Solid Mech. Arch., vol. 9, no. 3, 1984, pp. 259–267.

154. Bialkiewicz, J.: "Dynamic Creep Rupture of a Rotating Disk of Variable Thickness," Int. J. Mech. Sci., vol. 28, no. 10, 1986, pp. 671–681.

155. Gurvich, M.R.: "Stress-Strain and Limit State Viscoelastic Chord Flywheel," Probl. Prochn., vol. 6, 1987, pp. 7–11.

156. Antsilevich, Ya.G.: "Creep Rupture Strength of Composite Shell in The Field of Centrifugal Forces," Probl. Prochn., no. 6, 1991, pp. 62–66.

157. Trufanov, N.A. and Smetannikov, O.Yu: "Creep of Composite Energy Accumulators," Strength of Mater, vol. 23, no. 6, 1992, pp. 671–675.

158. Betten, J. and Shin, C.H.: "Inelastic Behavior of Rotating Disks Considering Effects of Anisotropy and Tensorial Nonlinearity," Forsch Ingenieurwes, vol. 57, no. 5, 1991, pp. 137–147.

159. Gotoh, J.; Misawa, A.; Takashi, M.; and Kunio, T.: "Periodic Wear Generated on Rotating Viscoelastic Disk with Point Contact," Nippon Kikai Gakkai Ronbunshu A Hen, vol. 60, no. 572, 1994, pp. 1005–1010.

160. Muthuswamy, V.P. and Mohan, S.R.: "Study of Fracture in a Rotating Disk," Def. Sci. J., vol. 24, no. 4, 1974, pp. 139–144.

161. Shiratori, E.; Ikegami, K.; Hattori, T.; and Shimizu, K.: "Application of the Fiber Reinforced Composite to Rotating Disks," Bull JSME, vol. 18, no. 122, 1975, pp. 784–796.

162. Bindin, P.J.: "Finite Element Study of a Cast Iron Flywheel with Particular Emphasis on Stress Concentrations," John Wiley and Sons, pp. 75–89.

163. Sakata, M.; Aoki, S.; Kishimoto, K.; Kanzawa, M.; and Ogure, N.: "Crack Growth and Unstable Fracture of Rotating Disk," J. Eng. Mater. Technol. Trans. ASME, vol. 107, no. 2, 1985, pp. 154–160.

164. Smith, R.N.L.: "Stress Intensity Factors for an Ark Crack in a Rotating Disk," Eng. Fract. Mech., vol. 21, no. 3, 1985, pp. 579–587.

165. Ezumi, T. and Takahashi, S.: "Photoelastic Experiment on the Stress-Intensity Factors for the Mixed Model in Rotating Disks," Nippon Kikai Gakkai Ronbunshu A Hen, vol. 52, no. 480, 1986, pp. 1885–1890.

166. Sukere, A.A.: "Stress Intensity Factors of Internal Radial Cracks in Rotating Disks by the Method of Caustics," Eng. Frac. Mech., vol. 26, no. 1, 1987, pp. 65–74.

167. Schneider G.A. and Danzer, R.: "Calculation of Stress Intensity Factor of an Edge Crack in a Finite Elastic Disk Using the Weight Function Method," Eng. Fract. Mech., vol. 34, no. 3, 1989, pp. 547–552.

168. Gregory, R.D.: "Spinning Circular Disk with a Radial Edge Crack; an Exact Solution," Int. J. Fract., vol. 41, no. 1, 1989, pp. 39–50.

169. Gau, C. and Nicholson, D.W.: "Finite Element Analysis of Crack-Tip Stress Intensity Factors in Steadily Rotating Disks," ASME Pet Div. Publ PD, vol. 29, 1990, pp. 161–169.

170. Chu, S.J. and Hong, C.S.: "Application of the Jk Integral to Arc Cracked Rotating Disks," Trans. Tech. Publ., Zuerich, Switz, 1991, pp. 391–396.

171. Theotokoglou, E.N.: "Integral Equation Solution of the Eccentrically Rotating Cracked Finite Elastic Disk," Eng. Fract. Mech., vol. 41, no. 2, 1992, pp. 299–308.

172. Xu, Y.L.: "Stress Intensity Factor of a Radial Crack in a Rotating Compound Disk," Eng. Fract. Mech., vol. 44, no. 3, 1993, pp. 409–423.

173. Bert, Ch.H. and Paul, T.K.: "Failure Analysis of Rotating Disk," Int. J. Solids. Struct., vol. 32, 1995.

174. Simpson, W.A. and McClung, R.W.: "Ultrasonic Detection of Fatigue Damage in Glass-Epoxy Composite Flywheels," ASTM, 1992, pp. 215–235.

175. Arnold, S.M.: "A Thermoelastic Transversely Isotropic Thick Walled Cylinder/Disk Application: An Analytical Solution and Study," NASA TM–102320, 1989.

176. Ugural A.C. and Fenster, S.K.: Advanced Strength and Applied Elasticity, Second SI Edition, 1987.

177. Jain, R.; Ramachandra, K.; and Simha, K.R.Y.: "Singularity in Rotating Orthotropic Disks and Shells," Int. J. Solids Struct., vol. 37, 2000, pp. 2035–2058.

178. Arnold, S.M., Bednarcyk, B.A.; Trowbridge, D.; and Wilt, T.E.: "Micromechanics Analysis Code with Generalized Method of Cells (MAC/GMC) User Guide: Version 3.0," NASA/TM—1999-209070, 1999.

179. Gabrys, C.W.; and Bakis, C.E.: "Design and Manufacturing of Filament Wound Elastomeric matrix Composite Flywheels," J. Reinf. Plast. Comp., vol. 16, no. 6, 1997.

180. Gates, T.S.; Chen, J.L.; and Sun, C.T.: "Micromechanical Characterization of Nonlinear Behavior of Advanced Polymer Matrix Composites," Compos, Mater., 1996, pp. 295–319.

181. Hexcel Corporation: Resin Vendor, http://www.hexcelcomposites.com/markets/aerospace/index.html

182. Ashby, M.: "Materials Selection In Mechanical Design," Butterworth & Heinemann, 2nd Edition, 1999.

183. Hill, R.: The Mathematical Theory of Plasticity," Oxford University Press, 1950.

184. Nadai, A.: Plasticity, McGraw Hill, 1931.

185. Robinson, D.N. and Pastor, M.S.: "Limit Pressure of a Circumferentially Reinforced SiC/Ti Ring," Compos. Eng., vol. 2, no. 4, 1992, pp. 229–238.

186. Robinson, D.N. and Duffy, S.F.: "Continuum Deformation Theory for High Temperature Metallic Composites," J. Eng. Mech., vol. 116, no. 4, 1990, pp. 832–844.

187. Saleeb, A.F. and Arnold, S.M.: "Limit Load Calculations for Rotating Anisotropic Disks/Cylinders," in preparation, 2000.

188. Arnold, S.M. and Kruch, S.: "Differential Continuum Damage Mechanics Models for Creep and Fatigue of Unidirectional Metal Matrix Composites," NASA TM–105213, 1991.

189. Arnold, S.M. and Kruch, S.: "A Differential CDM Model for Fatigue of Unidirectional Metal Matrix Composites," Int. J. Damage Mech., vol. 3, no. 2, 1994, pp. 170–191.

190. Wilt, T.E. and Arnold, S.M.: "A Coupled/Uncoupled Deformation and Fatigue Damage Algorithm Utilizing the Finite Element Method," NASA TM–106526.

191. Arnold, S.M. and Wilt, T.E.: "A Deformation and Life Prediction of a Circumferentially Reinforced SiC/Ti 15-3 Ring," Reliability, Stress Analysis, and Failure Prevention, Ed. R.J. Schaller, DE-vol 55, ASME, 1993, pp. 231–238.

192. Lerch, B. and Saltman, J.F.: "Tensile Determination of Sic/Ti-15-3 Laminates," Comp Mat: Fatigue and Fracture, ASTM STP 1156, 1993, pp. 161–175.

TABLE I.—ENERGY STORAGE TYPES (ref. 5)

Storage type	Specific energy, Wh/kg
Magnetic fields	
Superconducting coil	1-2
Elastic deformations:	
Steel spring	0.09
Natural rubber band	8.8
Electrochemical reaction	
Lead-acid battery	17.9
Nickel-cadmium battery	30.6
Kinetic energy	
Maraging steel flywheel	55.5
4340 steel flywheel	33.3
Composite flywheel	[a]213.8

[a]Using longitudinal strength of Kevlar without any shape factor.

TABLE II.—ROTATING DISKS COMPSED OF ISOTROPIC MATERIALS

Conditions/type of study	Analytical	Numerical	Experimental
Variable thickness	[5], [6], [7], [16], [17], [20], [22], [23], [26], [32], [44], [55],	[8], [12], [24], [30], [42], [49], [50],	[28], [31], [40],
Uniform thickness	[5], [6], [7], [16], [17], [18], [19], [20], [21], [22], [23], [25], [26], [32], [33], [36], [44], [45], [51], [55],	[8], [12], [24], [27], [30], [34], [35], [37], [38], [39], [41], [42], [43], [46], [47], [49], [50], [51], [53], [54],	[28], [31], [40],
Misfit		[41],	
Temp	[18], [48],	[39], [46],	[31],

TABLE III.—ROTATING DISKS COMPOSED OF ANISOTROPIC MATERIALS

Conditions/type of study	Analytical	Numerical	Experimental
Variable thickness	[59], [61], [64], [66], [71], [88],	[9], [10], [107], [109], [116],	
Uniform thickness	[5], [56], [57], [58], [59], [60], [61], [62],[63], [64], [66], [67], [68], [69], [70], [71], [73], [75], [76], [88], [92], [95], [101], [103], [113].	[65], [72], [74], [77], [82], [84], [94], [98], [100], [104], [105], [106], [107], [108], [109], [110], [114], [116],	[60], [74], [75], [78], [79], [80], [81], [83], [85], [86], [87], [89], [90], [91], [93], [96], [97], [99], [102], [110], [112], [114],
Misfit	[5], [70],	[94], [111],	[90],
Temp	[61], [67],	[74], [82], [100], [108],	[74], [99].

TABLE IV.—NON-LINEAR ANALYSIS CLASSIFICATION FOR ROTATING DISKS

Conditions/type of study	Isotropic	Anisotropic
Elasto-Plastic		
Variable thickness	[136],	[127]
Uniform thickness	[119], [120], [121], [122], [123], [124], [128], [129], [130], [131], [132], [133], [137], [138], [139], [141]	
Temp	[118], [125], [126], [134], [135], [140].	
Creep/Viscoelastic		
Variable thickness	[143], [151], [155]	
Uniform thickness	[141], [142], [144], [146], [147], [148], [149], [154],	[150], [156] [157], [158], [159],
Temp	[143], [145], [151], [152], [153].	
Fracture		
Variable thickness		
Uniform thickness	[160], [162], [163], [164], [165], [166], [168], [169], [171], [172], [173]	[161], [170]
Temp	[167],	
Fatigue		
Variable thickness		
Uniform thickness		[174]
Temp		

TABLE V.—SUMMARY OF PROBLEMS INVESTIGATED TO VALIDATE
PRESENT ANALYTICAL SOLUTION.

Type/Alternate Method	Rotation	Pressure	Thermal	Misfit
Solid Anisotropic Disk				
FEA	X	X	X	
Single Annular Anisotropic Disk				
Lekhnitskii [58] & FEA	X			
Arnold [175]		X	X	
Hub/Anisotropic Disk				
FEA			X	X
Two Annular, isotropic Disks				
Ugural and Fenster [176]				X

TABLE VI.—ROOM TEMPERATURE PMC MATERIAL PROPERTY DATA

Property	Fiber, (ref. 180)	Resin, (ref. 181)	v_f = 40 percent	v_f = 60 percent	v_f = 80 percent
E_L, Msi	40.0	0.677	16.4	23.1	32.1
E_T, Msi	2.0	0.677	1.06	1.26	1.58
v_L	0.25	0.33	0.295	0.282	0.267
v_T	0.25	0.33	0.42	0.373	0.303
G_L, Msi	2.9	0.2544	0.425	0.62	1.5
α_L, in./in./°F	-0.22×10^{-06}	42.0×10^{-06}	0.845×10^{-06}	0.269×10^{-06}	-0.032×10^{-06}
α_T, in./in./°F	6.28×10^{-06}	42.0×10^{-06}	33.7×10^{-06}	25.4×10^{-06}	17.0×10^{-06}
ρ, kip-sec^2/in^4	1.6511×10^{-07}	1.2163×10^{-07}	1.3033×10^{-07}	1.477×10^{-07}	1.5657×10^{-07}
UTS, Ksi	747 to 790	17.5	[a]110	[a]302 L [b]10 T	[a]398

[a]Determined via rule of mixture with a 0.3 knockdown for in-situ strength.
[b]Suggested from experiment.

TABLE VII.—ROOM TEMPERATURE TMC MATERIAL PROPERTY DATA

Property	Fiber SCS-6. (ref. 192)	Matrix Ti-15-3. (ref. 192)	SCS6/Ti-15-3 v_f =15 percent	SCS6/Ti-15-3 v_f =35 percent, (ref. 192)		SCS6/Ti-15-3 v_f =55%
E_L, Msi	58	13.0	19.8	28.8	**26.1**	37.8
E_T, Msi	58	13.0	15.7	20.2	**17.4**	27.0
v_L	0.19	0.33	0.306	0.272		0.249
v_T	0.19	0.33	0.366	0.37		0.319
G_L, Msi	24.36	4.924	5.65	7.0		9.62
α_L, in/in/°C	2.2×10^{-06}	8.1×10^{-06}	5.54×10^{-06}	3.99×10^{-06}		3.18×10^{-05}
α_T, in/in/°C	2.2×10^{-06}	8.1×10^{-06}	7.66×10^{-06}	6.38×10^{-06}		5.24×10^{-06}
ρ, kip-sec^2/in^4	3.085×10^{-07}	4.21×10^{-07}	4.04×10^{-07}	3.81×10^{-07}		3.591×10^{-07}
UTS, Ksi	550 to 650	126.2	[a]185	[a]257	201.6 L 60.9 T	[a]347

[a]Determined via rule of mixture: Bolded values are experimentally measured, (ref. 192).

TABLE VIII.—MAXIMUM NORMALIZED RADIAL AND TANGENTIAL STRESS FIELDS

R_m	$\sigma_r/\rho\omega^2 = g(\beta, R_m, \lambda)\,b^2$						$\sigma_\theta/\rho\omega^2 = f(\beta, R_m, \lambda)\,b^2$					
	$\lambda=2$		$\lambda=4$		$\lambda=8$		$\lambda=2$		$\lambda=4$		$\lambda=8$	
	PMC	TMC	PMC	TMC	PMC	TMC	PMC	TMC	PMC	TMC	PMC	TMC
4	1.08	1.6	2.1	6.3	3.8	19.5	17.8	22.0	22.	29.	39.	25
8	1.46	1.64	4.3	6.5	8.5	25.1	72.8	75.3	71	88	88	116
16	1.6	1.65	5.8	6.6	17.4	26.1	276	278	291	301	286	353
32	1.64	1.65	6.4	6.5	23.4	26.3	1066	1067	1106	1111	1165	1205

TABLE IX.—DESCRIPTION OF MATERIAL GRADATION BY CASE

Case	Disk 1	Disk 2	Disk 3
One	v_f = 60%, PMC	v_f = 60%, PMC	v_f = 60%, PMC
Two	v_f = 20%, PMC	v_f = 60%, PMC	v_f = 80%, PMC
Three	v_f = 80%, PMC	v_f = 60%, PMC	v_f = 20%, PMC
Four	v_f = 35%, SCS-6/Ti-51-3	v_f = 35%, SCS-6/Ti-51-3	v_f = 35%, SCS-6/Ti-51-3
Five	v_f = 15%, SCS-6/Ti-51-3	v_f = 35%, SCS-6/Ti-51-3	v_f = 55%, SCS-6/Ti-51-3
Six	v_f = 55%, SCS-6/Ti-51-3	v_f = 35%, SCS-6/Ti-51-3	v_f = 15%, SCS-6/Ti-51-3

TABLE X.—MAXIMUM SPECIFIC STORED ENERGY (KJ/KG) FOR A SINGLE DISK MADE WITH PMC

Criterion	Annular Disk Case (λ = 3)				Solid Disk Case (a = 0)			
	$R_m = 4$[a]	$R_m = 8$	$R_m = 16$	$R_m = 32$	b = 5.5	b = 9.5	b = 17.5	b = 33.5
Hoop Only								
v_f = 40%	327.86	295.29	299.96	313.04	275.62	275.67	275.74	275.79
v_f = 60%	792.16	713.46	724.75	756.37	665.94	666.06	666.23	666.36
v_f = 80%	983.93	886.17	900.19	939.46	827.14	827.29	827.51	827.67
Radial Only								
v_f = 40%	113.74	250.12	825.3	3127.1	87.285	87.357	87.514	87.64
v_f = 60%	267.56	588.40	1942.1	7357.1	205.34	205.51	205.88	206.17
v_f = 80%	338.8	745.05	2458.1	9316.1	260.01	260.22	260.69	261.06
Multiaxial								
v_f = 40%	115.36	211.14	299.96	313.04	89.848	90.048	90.109	90.01
v_f = 60%	278.72	510.15	724.75	756.37	217.09	217.57	217.72	217.48
v_f = 80%	346.19	633.65	900.19	939.46	269.64	270.24	270.42	270.12

[a]R_m, b and λ has the units of inches.

TABLE XI.—MAXIMUM SPECIFIC STORED ENERGY (KJ/KG) FOR A SINGLE
DISK MADE WITH TMC

Criterion	Annular Disk Case ($\lambda = 3$)				Solid Disk Case (a = 0)			
	$R_m = 4^a$	$R_m = 8$	$R_m = 16$	$R_m = 32$	b = 5.5	b = 9.5	b = 17.5	b = 33.5
Hoop Only								
$v_f = 15\%$	105.53	119.76	131.69	139.10	190.68	190.75	190.68	190.69
$v_f = 35\%$	155.24	176.18	193.74	204.63	280.51	280.61	280.50	280.53
$v_f = 55\%$	222.74	252.79	277.97	293.60	402.48	402.62	402.46	402.50
Radial Only								
$v_f = 15\%$	225.36	802.10	3119.1	12361.0	72.94	72.97	72.94	72.97
$v_f = 35\%$	332.41	1183.10	4610.0	18231.0	107.58	107.64	107.58	107.63
$v_f = 55\%$	452.87	1612.10	6267.1	24831.0	146.56	146.64	146.57	146.63
Multiaxial								
$v_f = 15\%$	105.53	119.76	131.69	139.1	71.79	71.8	71.79	71.84
$v_f = 35\%$	155.24	176.18	193.74	204.63	105.61	105.62	105.62	105.69
$v_f = 55\%$	222.74	252.79	277.97	293.6	151.53	151.54	151.54	151.64

$^a R_m$, b and λ has the units of inches.

TABLE XII.—RATIO OF ANNULAR DISK TO SOLID DISK MAXIMUM SPECIFIED STORED
ENERGY

$\left(\dfrac{U}{m}\right)_A / \left(\dfrac{U}{m}\right)_s$	PMC ($\lambda = 3$)				TMC ($\lambda = 3$)			
	$R_m = 4^a$	$R_m = 8$	$R_m = 16$	$R_m = 32$	$R_m = 4$	$R_m = 8$	$R_m = 16$	$R_m = 32$
Criterion								
Hoop Only	1.19	1.071	1.088	1.135	0.553	0.628	0.691	0.729
Radial Only	1.303	2.863	9.43	35.686	3.09	10.991	42.758	169.359
Multiaxial	1.284	2.345	3.329	3.478	1.47	1.668	1.834	1.936

$^a R_m$ and λ has the units of inches.

TABLE XIII.—RATIO PMC TO THAT OF TMC
FLYWHEELS SPECIFIC ENERGY

$\left(\dfrac{U}{m}\right)_{PMC} / \left(\dfrac{U}{m}\right)_{TMC}$	Annular Disk Cases ($\lambda = 3$)			
	$R_m = 4^a$	$R_m = 8$	$R_m = 16$	$R_m = 32$
Hoop Only				
40%/15%	3.107	2.466	2.278	2.25
60%/35%	5.103	4.05	3.741	3.696
80%/55%	4.417	3.506	3.238	3.2
Radial Only				
40%/15%	0.505	0.312	0.265	0.253
60%/35%	0.805	0.497	0.422	0.404
80%/55%	0.748	0.462	0.392	0.375
Multiaxial				
40%/15%	1.093	1.763	2.278	2.25
60%/35%	1.795	2.896	3.741	3.696
80%/55%	1.554	2.507	3.238	3.2

$^a R_m$ and λ has the units of inches.

TABLE XIV.—COMPARISON OF BRITTLE AND
DUCTILE LIMITS

b/a = 1.35, ζ=0.93	Limit pressure, Ksi	Limit speed, rpm
Ductile	– – – –	– – – –
Upper Bound	61.038	55 320
Lower Bound	54.237	54 760
Brittle		
First Fracture (J_2)	39.1	51 180
First Fracture (σ_{max})	58.3	51 180
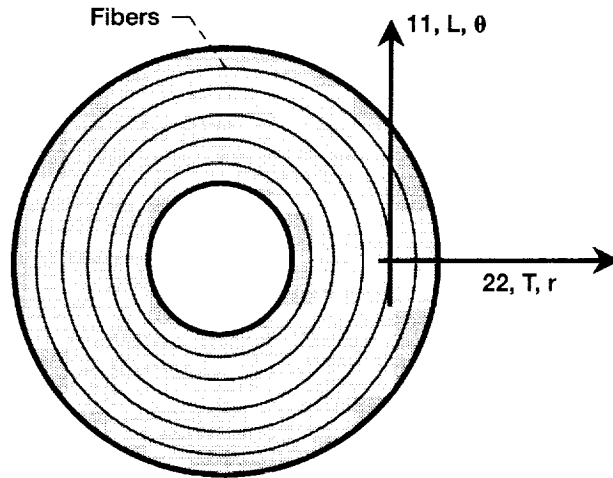
Figure 1.—Single disk, reinforced in the circumferential
direction.
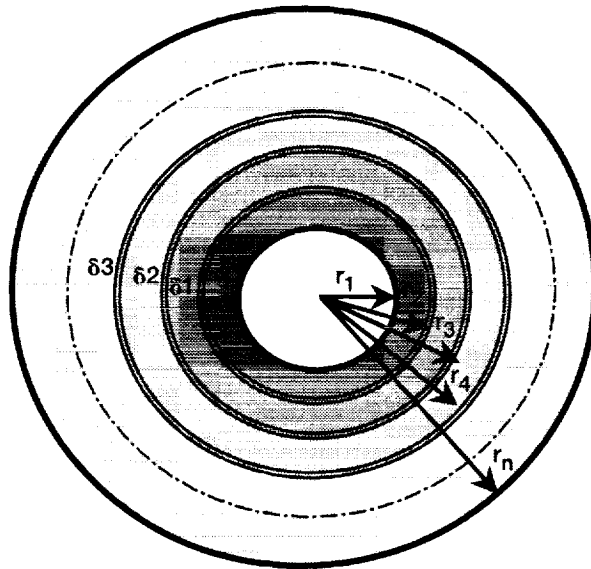
Figure 2.—Schematic of "n" concentric disks.
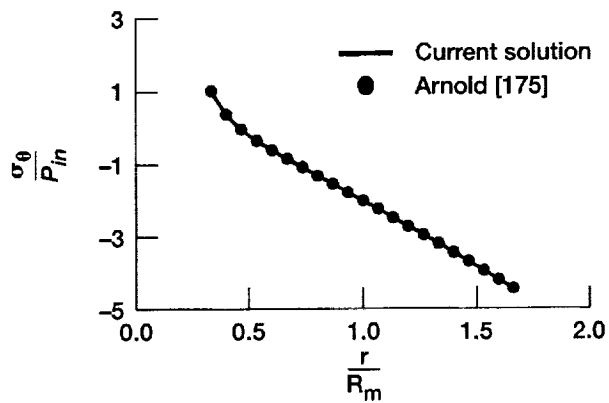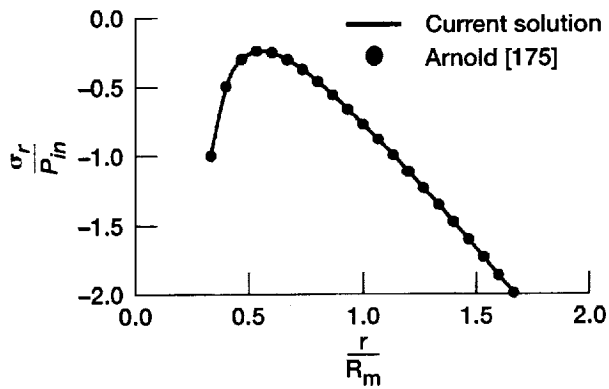
Figure 3.—Comparison between the current study and Arnold [175].
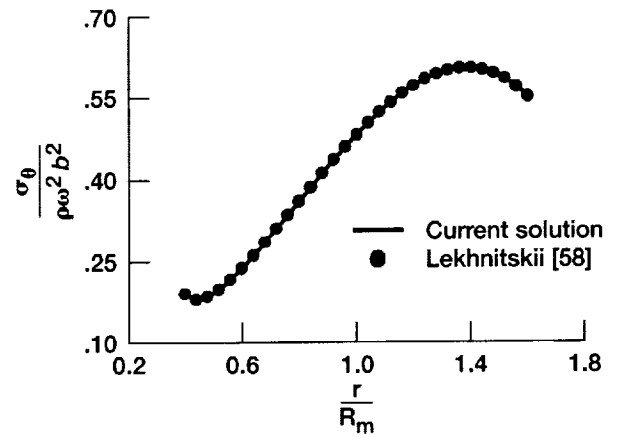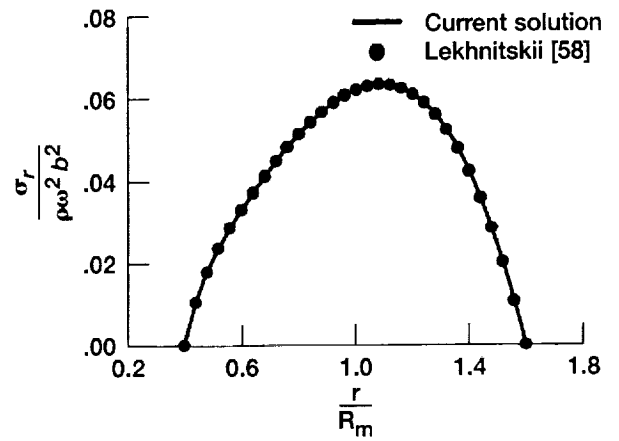
Figure 4.—Comparison between the current study and Lekhnitskii [58].
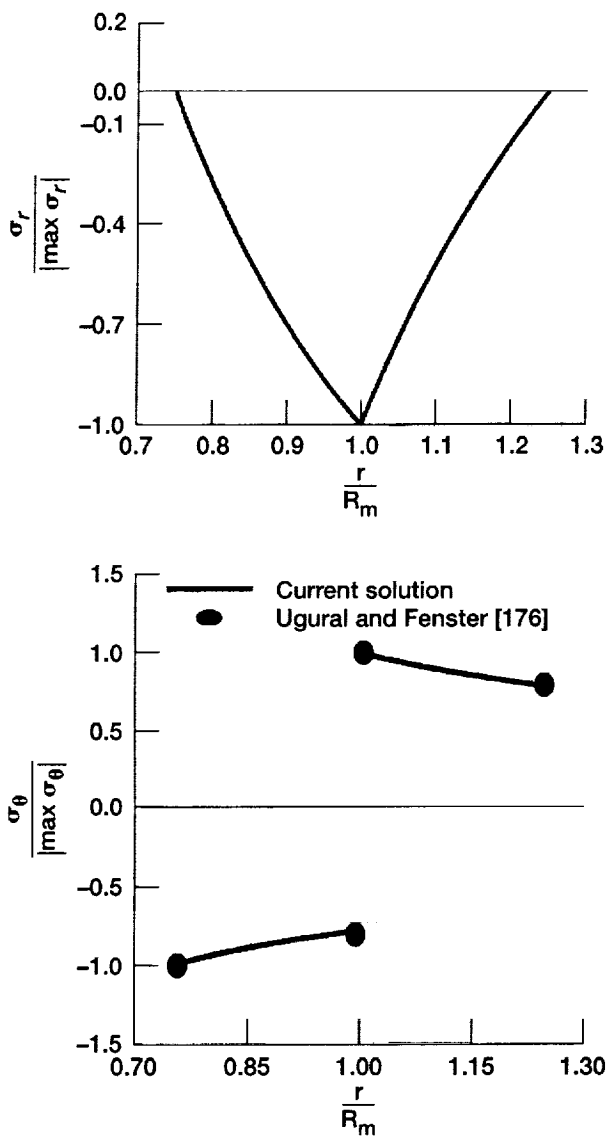
Figure 5.—Normalized radial and tangential stresses. Comparison with maximum given by Ugural and Fenster [176].
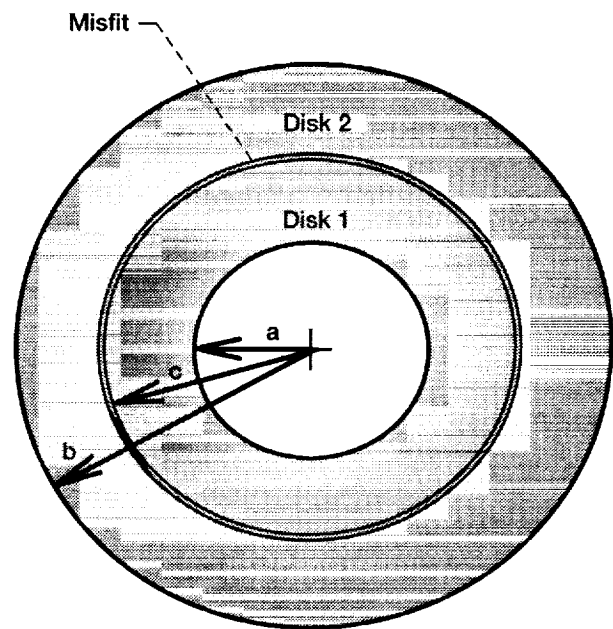
Figure 6.—Schematic representation of two concentric disks with misfit.
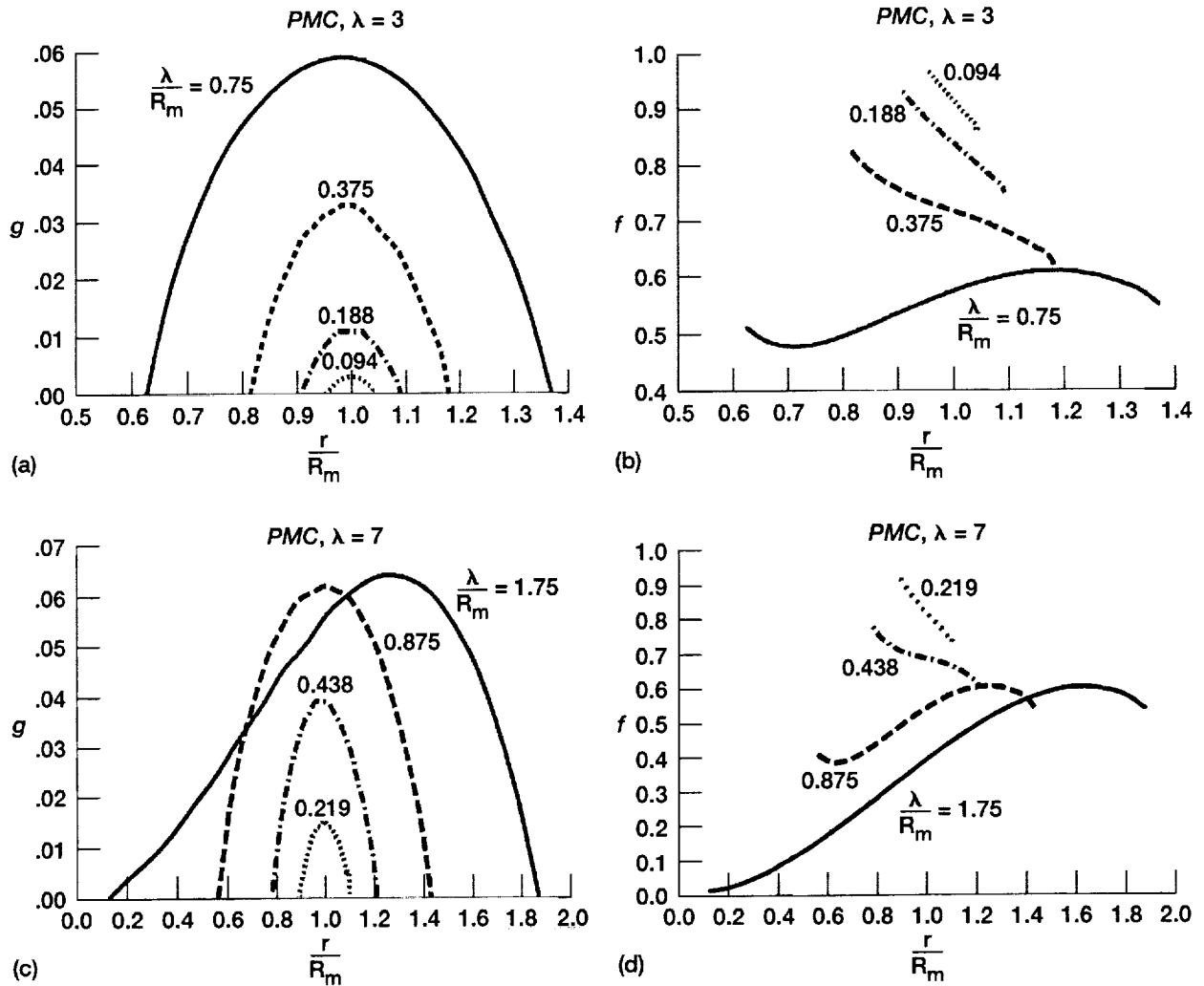
Figure 7.—Normalized radial "*g*" and tangential "*f*" stresses (aka distribution factors) versus normalized radius given a single rotating disk made from *PMC*. Figure (a) and (b) correspond to a 3 in. thick disk, while (c) and (d) to a 7 in. thick disk.
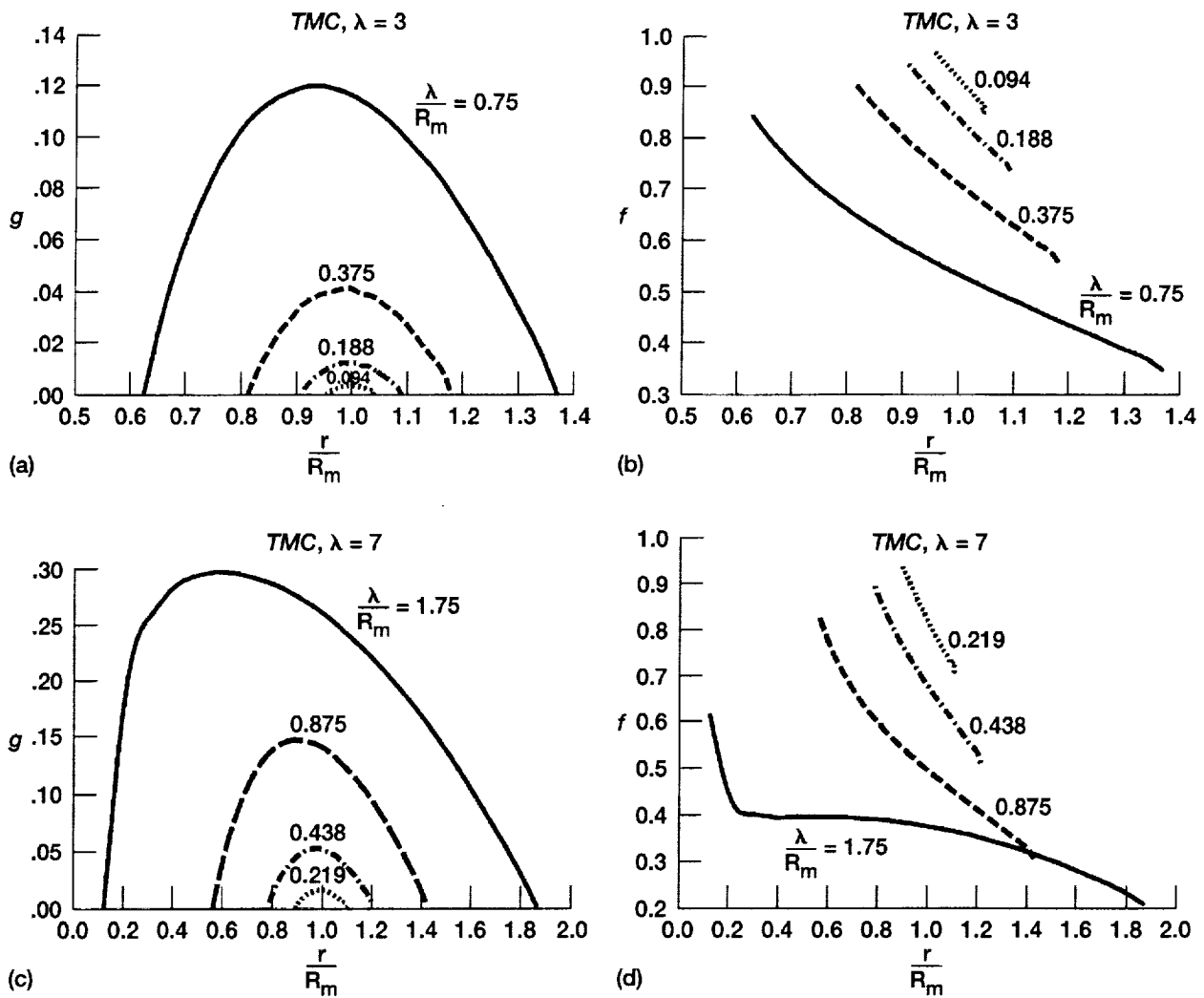
Figure 8.—Normalized radial "g" and tangential "f" stresses (aka distribution factors) versus normalized radius given a single rotating disk made from *TMC*. Figure (a) and (b) correspond to a 3 in. thick disk, while (c) and (d) to a 7 in. thick disk.
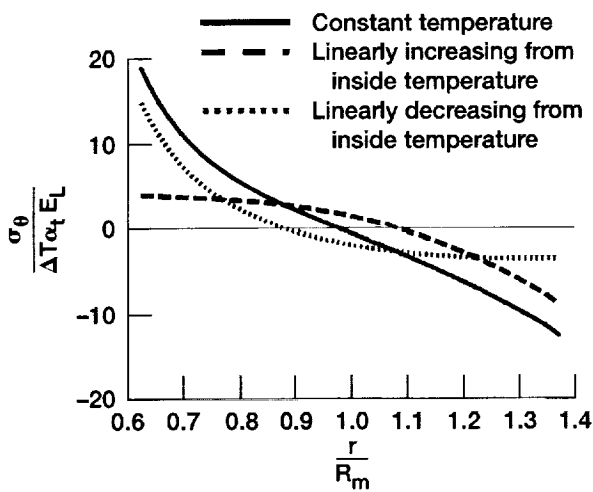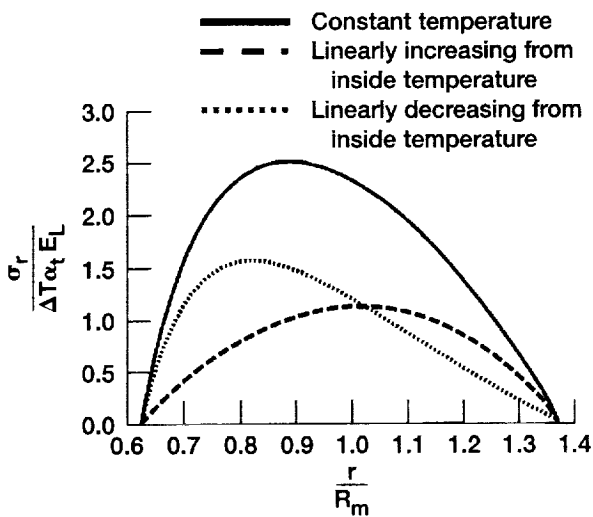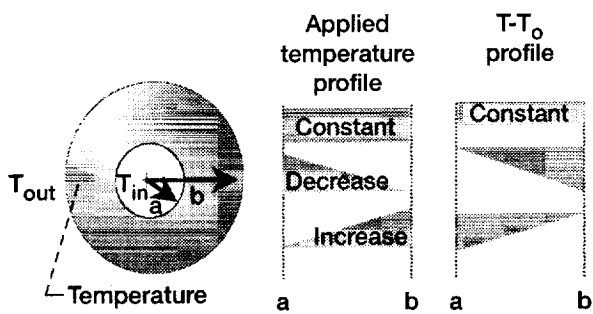
Figure 9.—Influence of temperature gradient on a single disk.
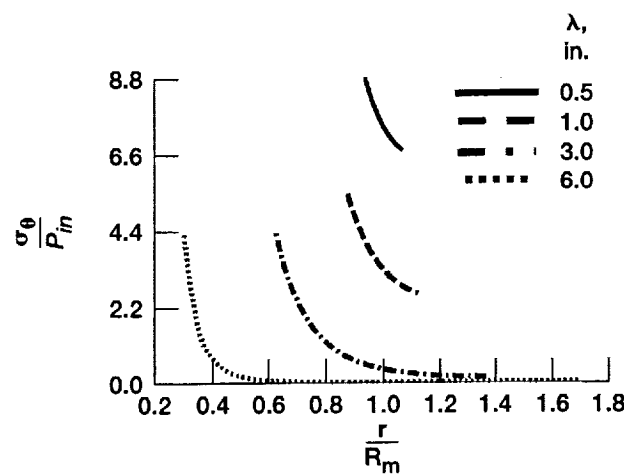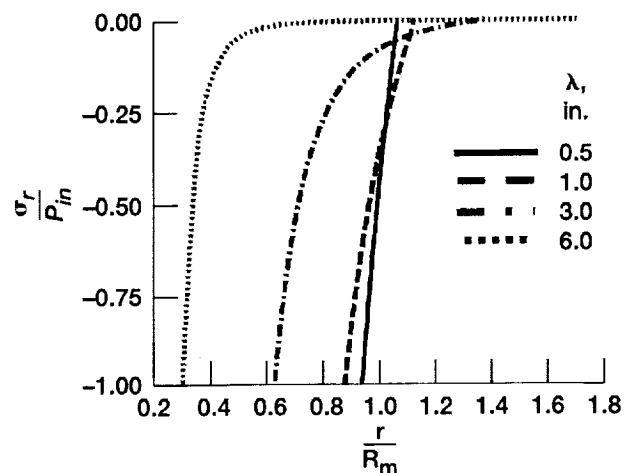
Figure 10.—Influence of applying pressure along the inner surface of a single disk. λ - thickness of disk.
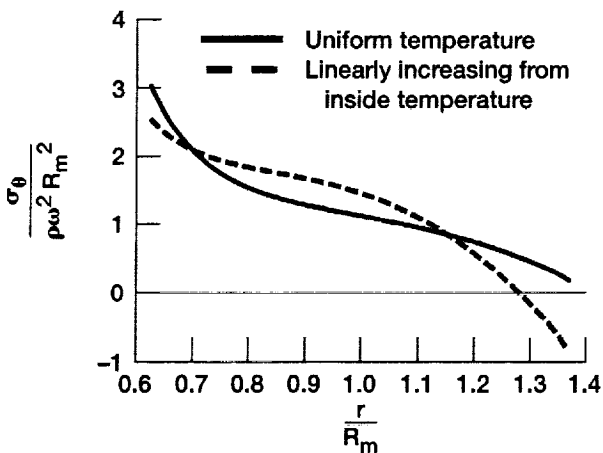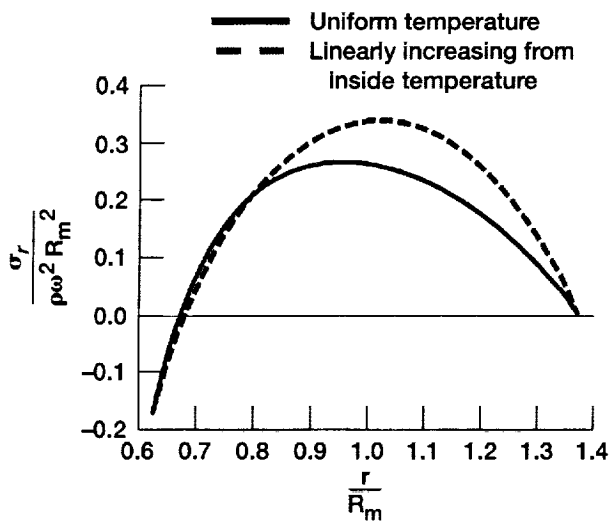
Figure 11.—Influence of thermal, internal pressure, and rotation on a single disk. Speed of rotation is 15 000 rpm.
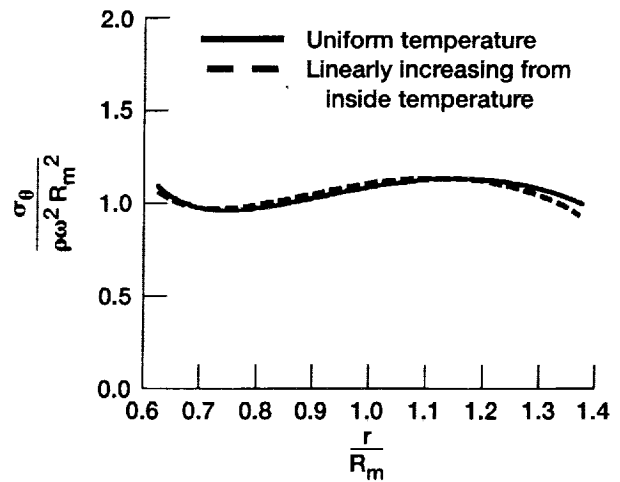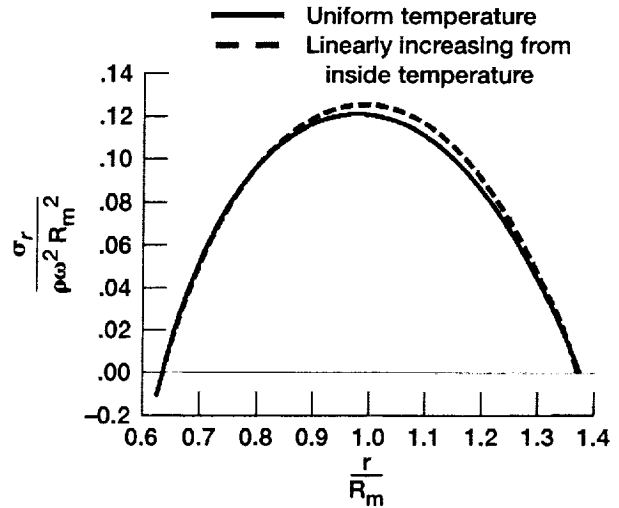
Figure 12.—Influence of thermal, internal pressure, and rotation on a single disk. Speed of rotation is 60 000 rpm.

(a)
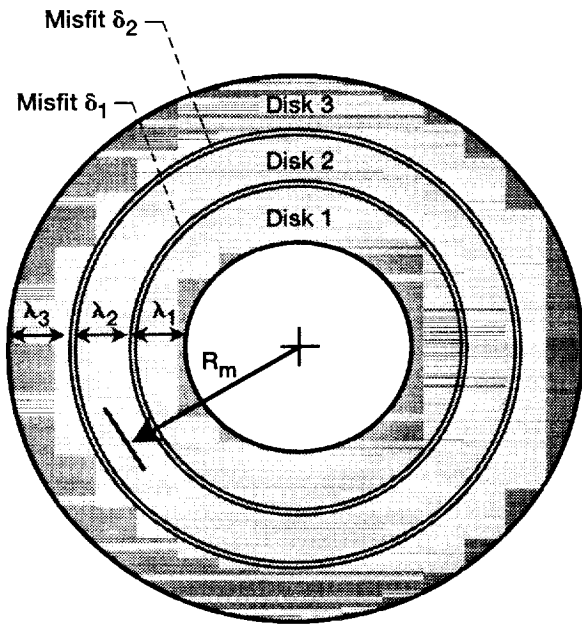
Figure 13.—Schematic representation of three concentric disks with misfit.
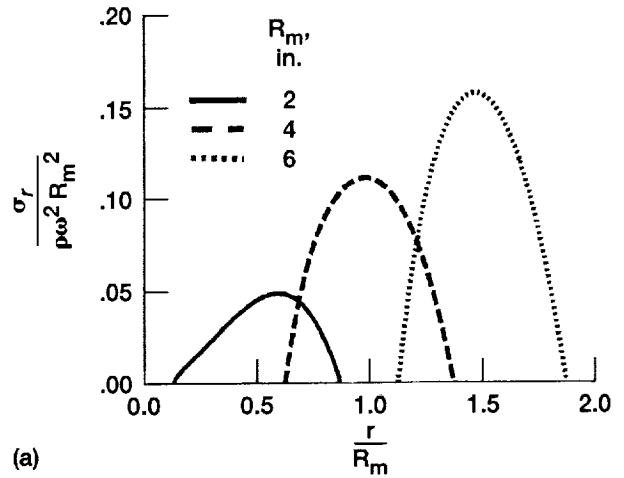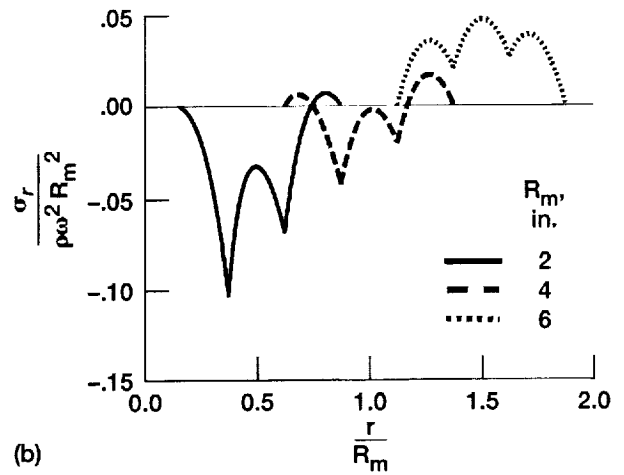
(b)
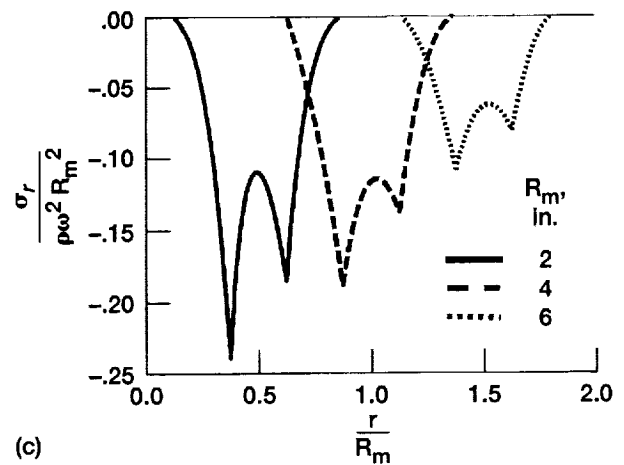
(c)

Figure 14.—Normalized radial stress for disk subjected to misfit and rotation. Case (a) has no misfit, i. e., $\varepsilon_h = 0$, (b) has $\varepsilon_h = 0.1\%$ and (c) has $\varepsilon_h = 0.2\%$ applied at all interfaces.
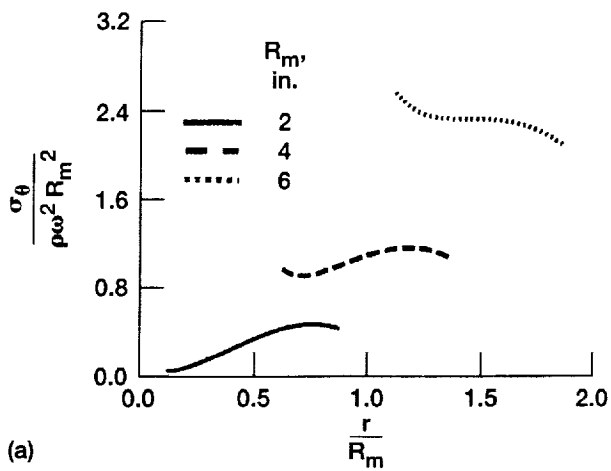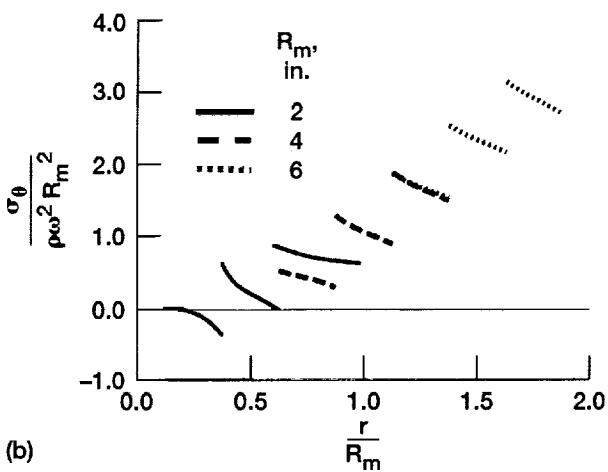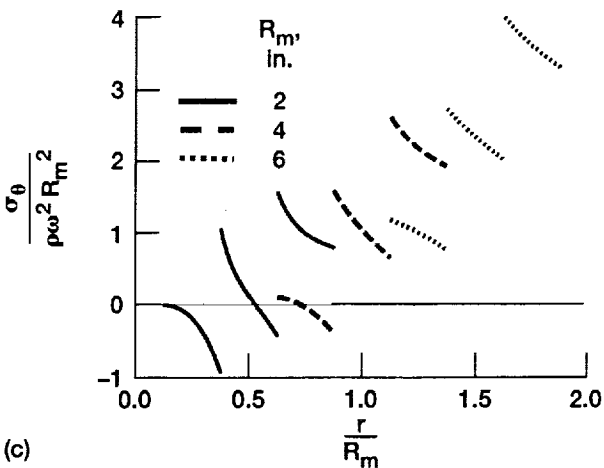
Figure 15.—Normalized tangential stress for disk sub-
jected to misfit and rotation. Case (a) has no misfit,
i. e., $\varepsilon_h = 0$, (b) has $\varepsilon_h = 0.1\%$ and (c) has $\varepsilon_h = 0.2\%$
applied at all interfaces.
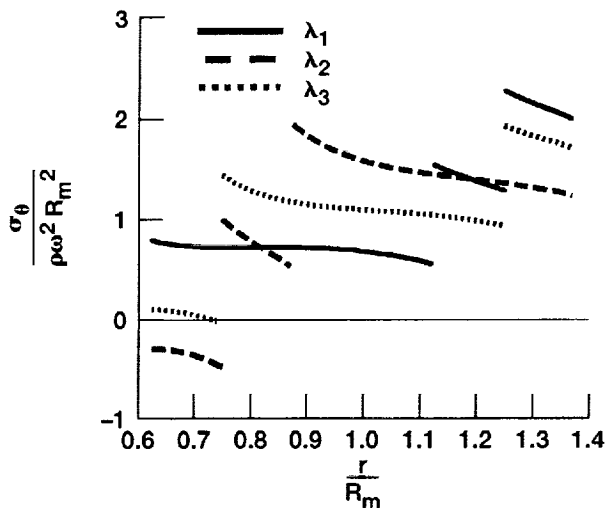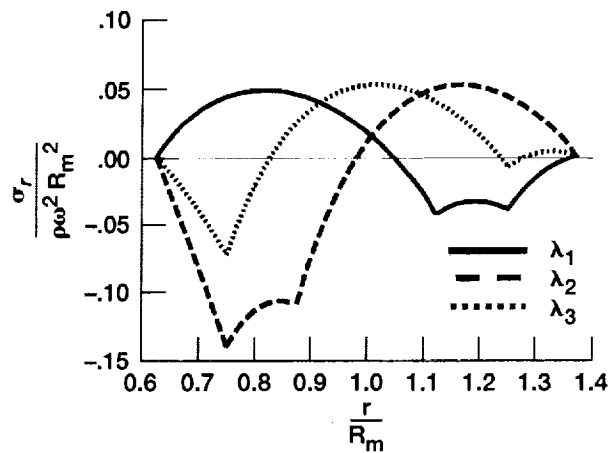
Figure 16.—Influence of varying internal disks
thickness on the radial and tangential stresses.
λ_1 {2, 0.5, 0.5}, λ_2 {0.5, 0.5, 2}, λ_3 {0.5, 2, 0.5}. The
misfit here is $\varepsilon_h = 0.1\%$.
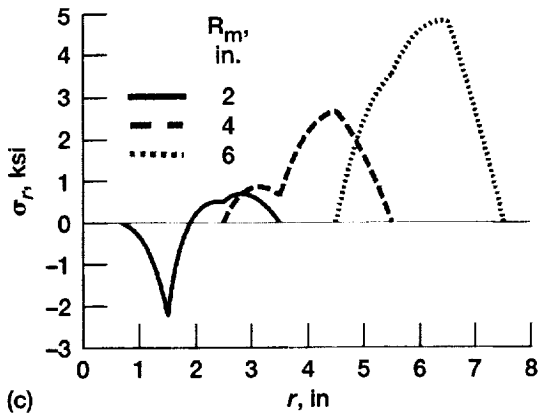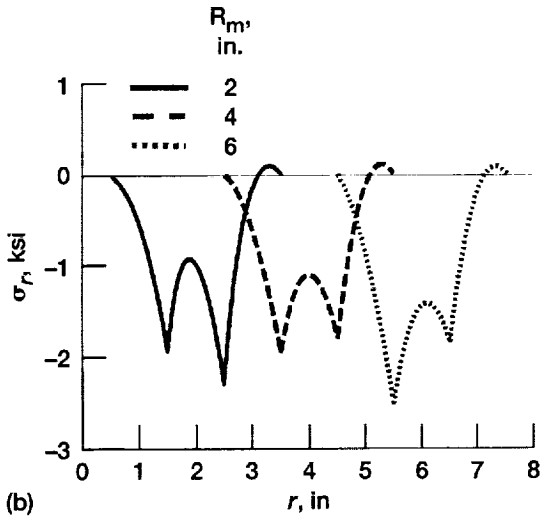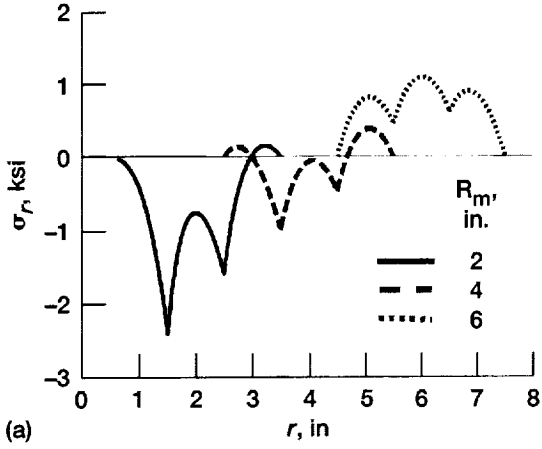
Figure 17.—Radial stress for different material configurations subjected to rotational speed of 30 000 rpm. (a) material case 1, (b) material case 2 and (c) material case 3. (see Table 9)
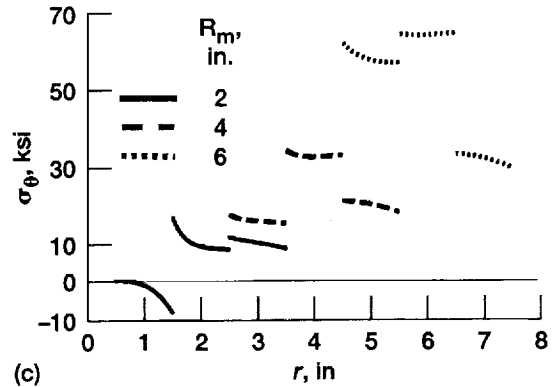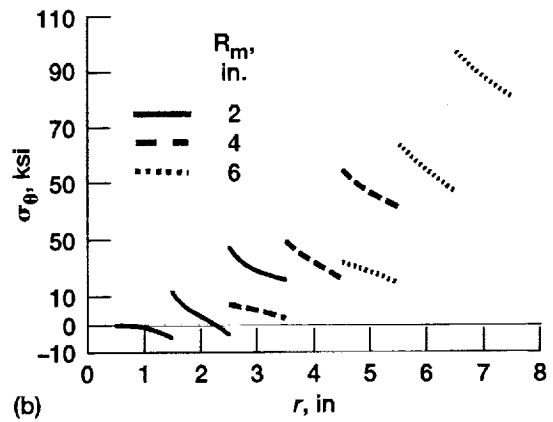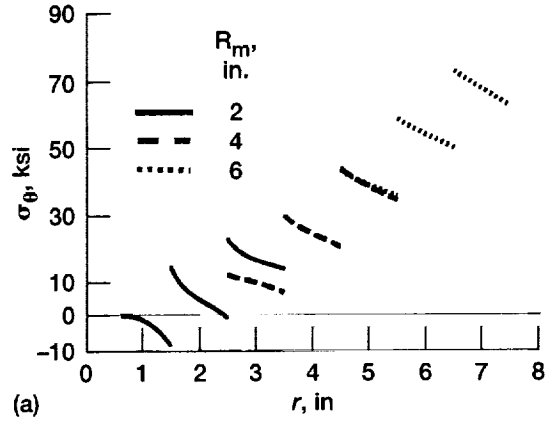

Figure 18.—Tangential stress for different material configurations subjected to rotational speed of 30 000 rpm. (a) material case 1, (b) material case 2 and (c) material case 3. (see Table 9).
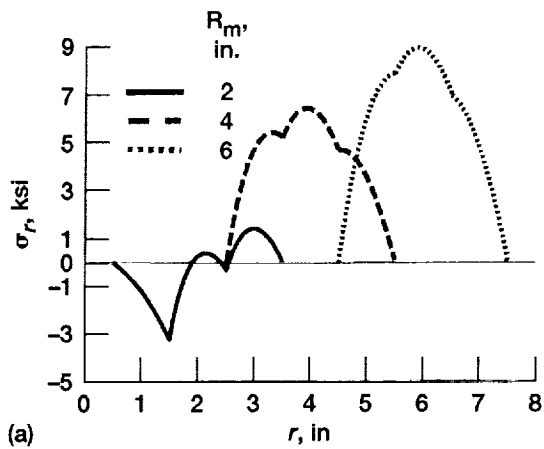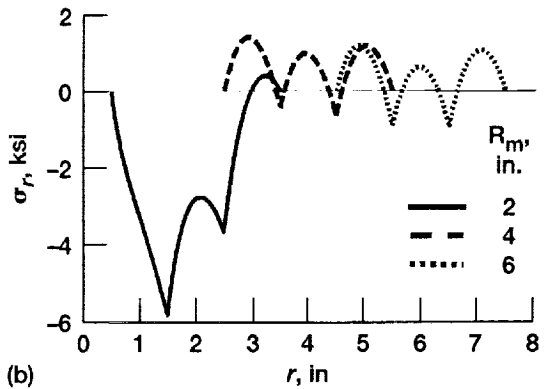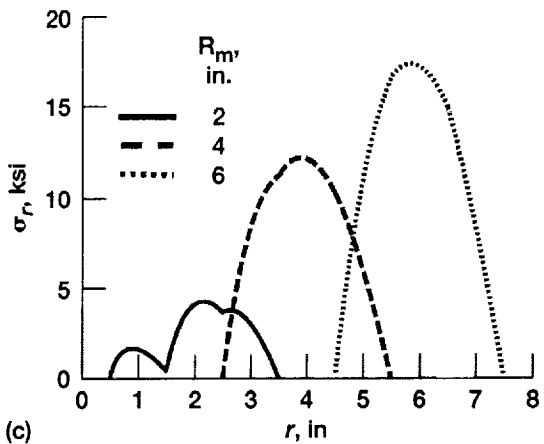
Figure 19.—Radial stress for different material
configurations subjected to rotational speed
of 30 000 rpm. (a) material case 4, (b) material
case 5 and (c) material case 6. (see Table 9).
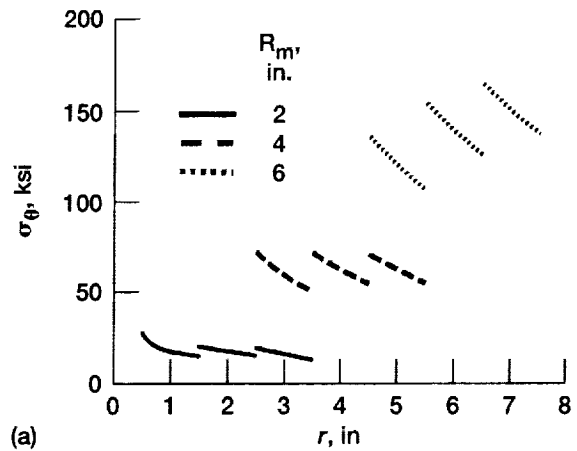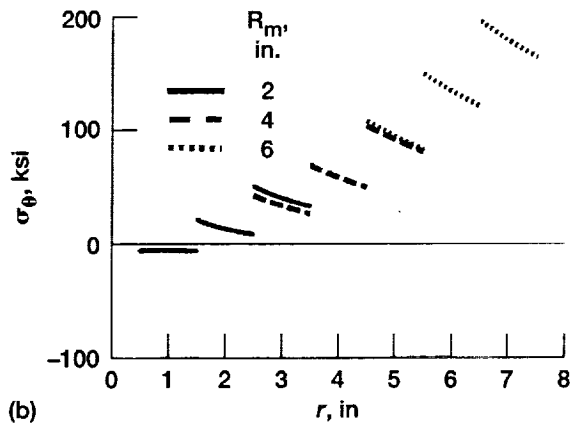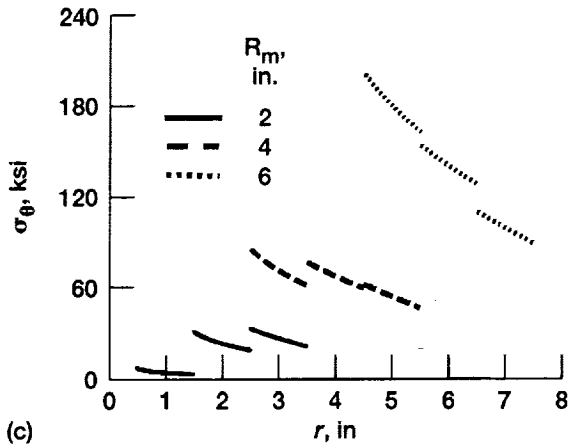
Figure 20.—Tangential stress for different material
configurations subjected to rotational speed of
30 000 rpm. (a) material case 4, (b) material
case 5 and (c) material case 6. (see Table 9).
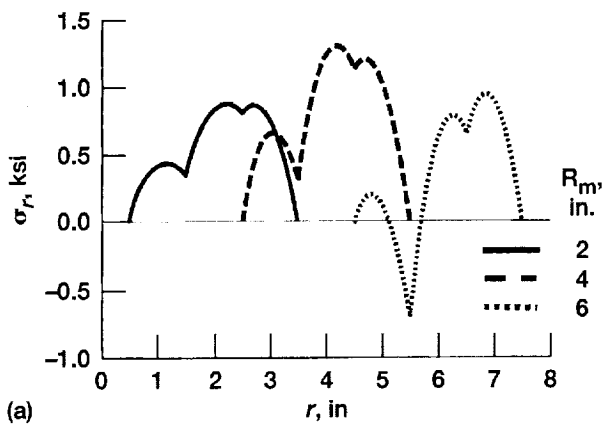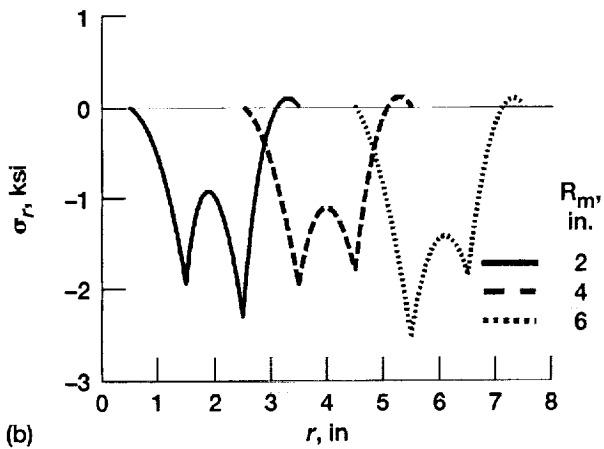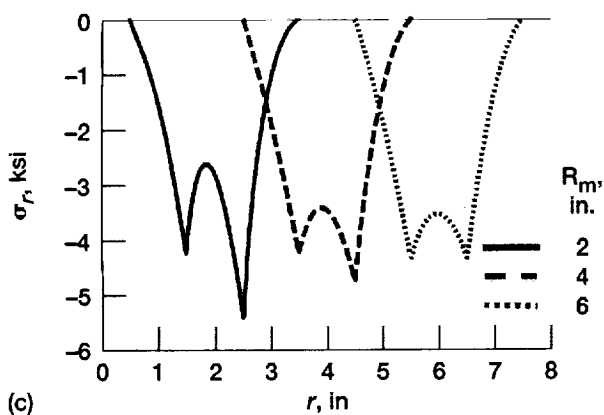
Figure 21.—Radial stress for material case 2 for different applied misfits subjected to rotational speed of 30 000 rpm. (a) $\varepsilon_h = 0$, (b) $\varepsilon_h = 0.1\%$ and (c) $\varepsilon_h = 0.2\%$.
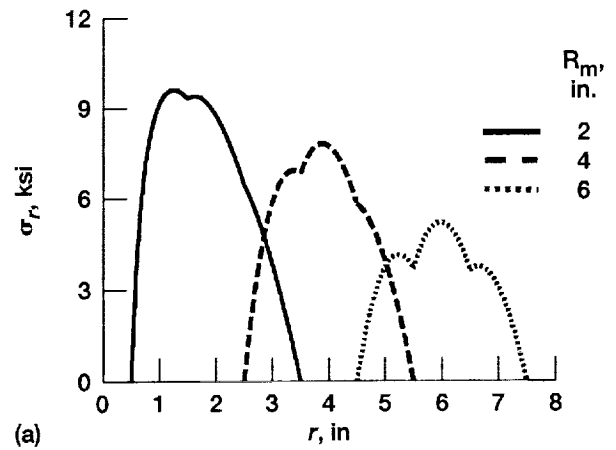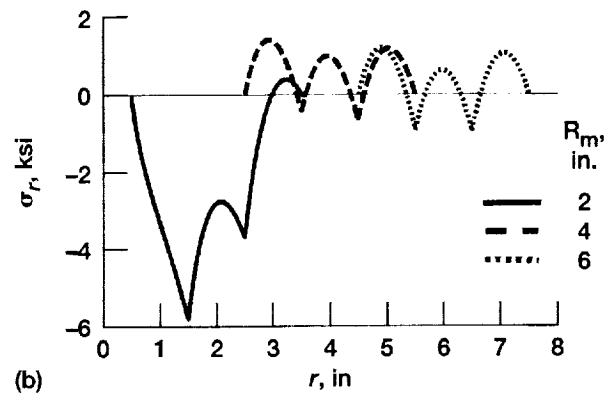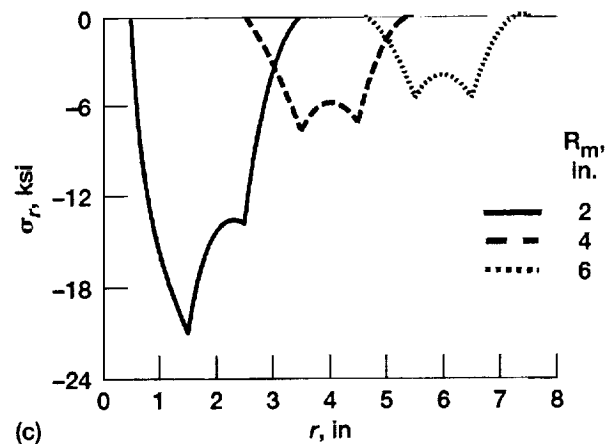
Figure 22.—Radial stress for material case 5 for different applied misfits subjected to rotational speed of 30 000 rpm. (a) $\varepsilon_h = 0$, (b) $\varepsilon_h = 0.1\%$ and (c) $\varepsilon_h = 0.2\%$.
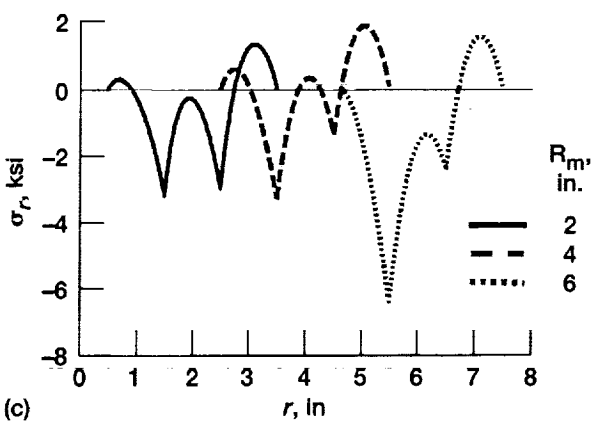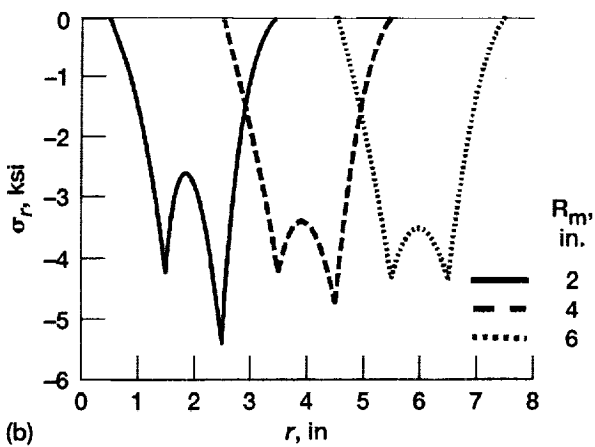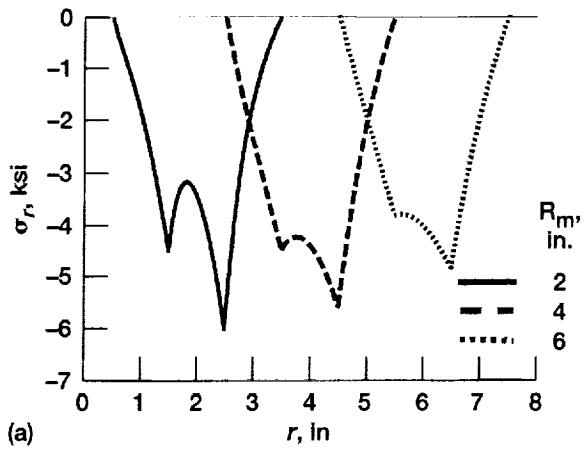
Figure 23.—Radial stress for material case 2 for different speeds of rotation. (a) ω = 15 000 rpm, (b) ω = 30 000 rpm, and (c) ω = 60 000 rpm.
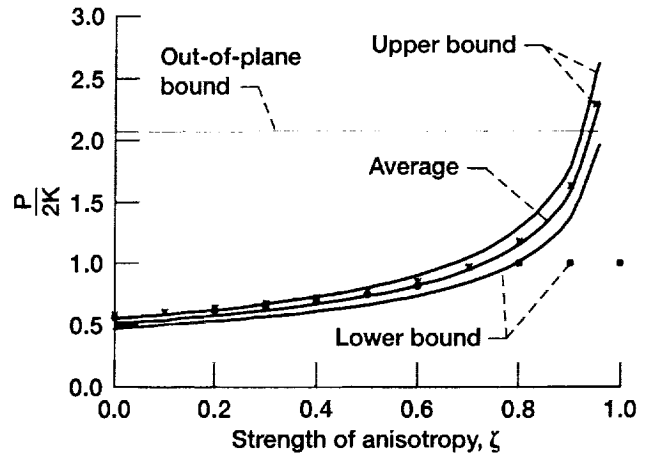
Figure 24.—Illustrates the upper and lower bounds for both rotation (solid lines) and internal pressure (symbols) limit loads by plotting the normalized effective pressure versus strength of anisotropy.
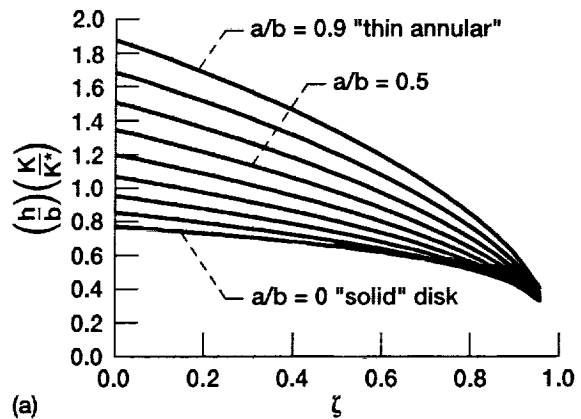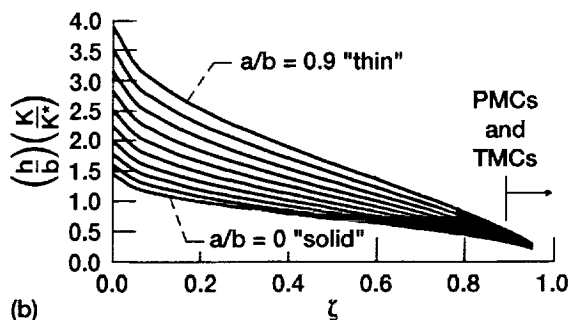

Figure 25.—Interaction curves for the out-of-plane failure bound: (a) represents the limit as compared to the in-plane lower bound, and (b) represents the limit as compared to the average in-plane bound. The h is the height of disk, b outer radius, ζ the strength of anisotropy.

(a) Mean radius affect
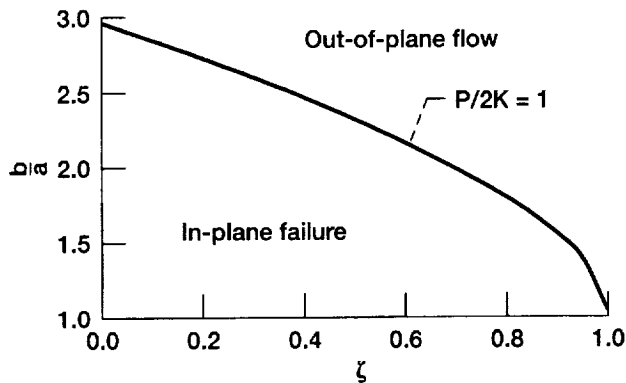
Figure 26.—Illustrates the interaction curve differentiating in-plane failure (below the line) and out-of-plane flow (on or above the line). $\frac{b}{a}$ is the ratio of outer to inner radius and ζ is a measure of the strength of anisotropy.
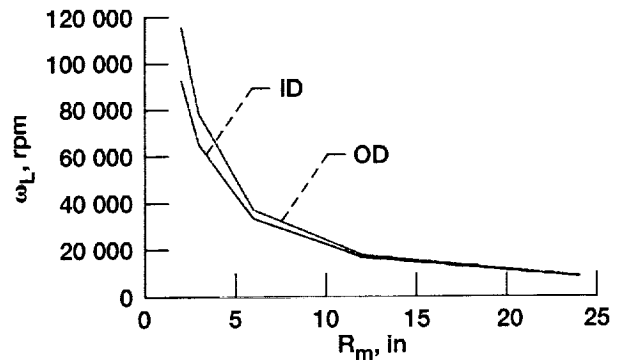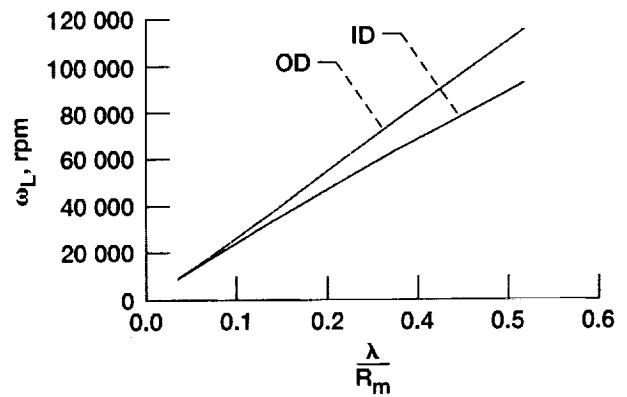
(b) Thickness affect

Figure 27.—Static limit or burst speed as a function of geometry, (a) maximum speed versus mean radius, (b) maximum speed versus the ratio of disk thickness to that of mean radius.

49
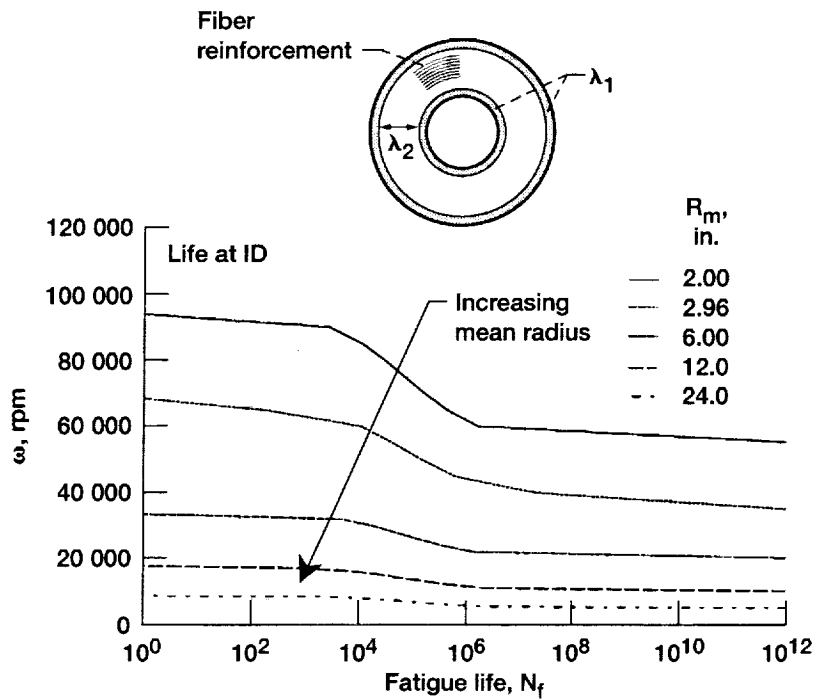
Figure 28.—Generalized speed versus cycles curve indicating the onset of fatigue initiation cracks at the inner radius of the composite core.
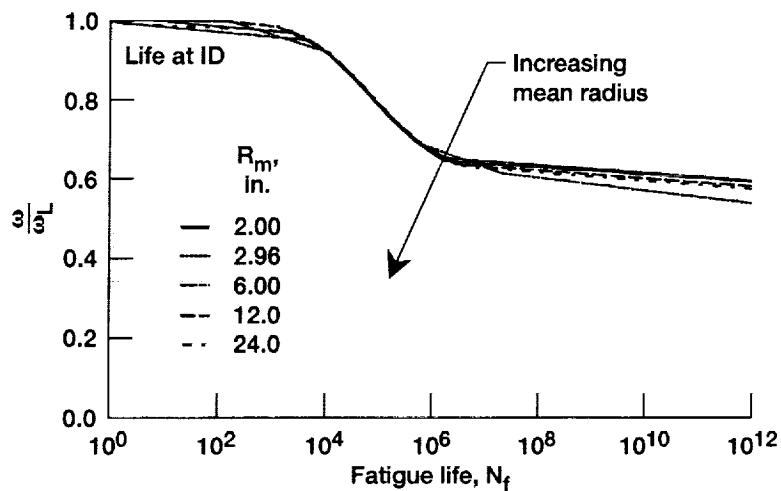

Figure 29.—Normalized speed versus cycle master curve denoting fatigue initiation at the inner diameter. ω_L is the static limit speed and ω is the maximum applied speed within a cycle.

REPORT DOCUMENTATION PAGE

Public reporting burden for this collection of information is estimated to average 1 hour per response, including the time for reviewing instructions, searching existing data sources, gathering and maintaining the data needed, and completing and reviewing the collection of information. Send comments regarding this burden estimate or any other aspect of this collection of information, including suggestions for reducing this burden, to Washington Headquarters Services, Directorate for Information Operations and Reports, 1215 Jefferson Davis Highway, Suite 1204, Arlington, VA 22202-4302, and to the Office of Management and Budget, Paperwork Reduction Project (0704-0188), Washington, DC 20503.

1. AGENCY USE ONLY (Leave blank)	2. REPORT DATE	3. REPORT TYPE AND DATES COVERED
	January 2001	Technical Memorandum

4. TITLE AND SUBTITLE

Deformation and Life Analysis of Composite Flywheel Disk and Multi-Disk Systems

6. AUTHOR(S)

S.M. Arnold, A.F. Saleeb, and N.R. Al-Zoubi

5. FUNDING NUMBERS

WU–755–A4–09–00
NCC3–788

7. PERFORMING ORGANIZATION NAME(S) AND ADDRESS(ES)

National Aeronautics and Space Administration
John H. Glenn Research Center at Lewis Field
Cleveland, Ohio 44135–3191

8. PERFORMING ORGANIZATION REPORT NUMBER

E–12547

9. SPONSORING/MONITORING AGENCY NAME(S) AND ADDRESS(ES)

National Aeronautics and Space Administration
Washington, DC 20546–0001

10. SPONSORING/MONITORING AGENCY REPORT NUMBER

NASA TM—2001-210578

11. SUPPLEMENTARY NOTES

12a. DISTRIBUTION/AVAILABILITY STATEMENT

Unclassified - Unlimited
Subject Categories: 24 and 39   Distribution: Nonstandard

Available electronically at http://gltrs.grc.nasa.gov/GLTRS

This publication is available from the NASA Center for AeroSpace Information, 301–621–0390.

12b. DISTRIBUTION CODE

13. ABSTRACT (Maximum 200 words)

In this study an attempt is made to put into perspective the problem of a rotating disk, be it a single disk or a number of concentric disks forming a unit. An analytical model capable of performing an elastic stress analysis for single/multiple, annular/solid, anisotropic/isotropic disk systems, subjected to both pressure surface tractions, body forces (in the form of temperature-changes and rotation fields) and interfacial misfits is derived and discussed. Results of an extensive parametric study are presented to clearly define the key design variables and their associated influence. In general the important parameters were identified as misfit, mean radius, thickness, material property and/or load gradation, and speed; all of which must be simultaneously optimized to achieve the "best" and most reliable design. Also, the important issue of defining proper performance/merit indices (based on the specific stored energy), in the presence of multiaxiality and material anisotropy is addressed. These merit indices are then utilized to discuss the difference between flywheels made from PMC and TMC materials with either an annular or solid geometry. Finally two major aspects of failure analysis, that is the static and cyclic limit (burst) speeds are addressed. In the case of static limit loads, upper, lower, and out-of-plane bounds for disks with constant thickness are presented for both the case of internal pressure loading (as one would see in a hydroburst test) and pure rotation (as in the case of a free spinning disk). The results (interaction diagrams) are displayed graphically in designer friendly format. For the case of fatigue, a representative fatigue/life master curve is illustrated in which the normalized limit speed versus number of applied cycles is given for a cladded TMC disk application.

14. SUBJECT TERMS

Deformation analysis; Elasticity; Misfit; Thermal; Mechanical; Rotating disk; Fatigue limit loads

15. NUMBER OF PAGES
56

16. PRICE CODE
A04

17. SECURITY CLASSIFICATION OF REPORT	18. SECURITY CLASSIFICATION OF THIS PAGE	19. SECURITY CLASSIFICATION OF ABSTRACT	20. LIMITATION OF ABSTRACT
Unclassified	Unclassified	Unclassified	